Archaeological and Anthropological Sciences (2026) 18:142
https://doi.org/10.1007/s12520-026-02453-1

RESEARCH

Reassessment and new evidence of the dental remains from Payre site (France)

Laura Martín-Francés[1,2] · Marina Martínez de Pinillos[1,3] · María Martinón-Torres[1,4] · Cecilia García-Campos[1,5] · Louise Magne[6] · Juan Luis Arsuaga[7,8] · José María Bermúdez de Castro[1] · Marie-Hélène Moncel[9] · Benoît Bertrand[6] · Amélie Vialet[9]

Received: 26 May 2025 / Accepted: 10 March 2026

Abstract

Morphological evidence suggests that European Middle Pleistocene hominins share a common phylogenetic history, yet they display a substantial morphometric variability. In particular, MIS 7−5 hominins have been proposed to exhibit a distinctive combination of traits differentiating them from both earlier and later Neanderthal populations. However, the scarcity of fossil remains from this period limits our understanding of Neanderthal evolutionary dynamics and regional variability. Here, we present a morphometric reassessment of the dental remains from Payre ($n=9$), combining external morphological descriptions, geometric morphometrics of the EDJ, and analysis of the dental tissue proportions. We test whether the Payre sample can be distinguished from earlier populations (e.g., Atapuerca-Sima de los Huesos) and from later Neanderthal groups (MIS 5−3), and we evaluate morphological variation across stratigraphic levels. Our results show that the Payre teeth align more closely with the MIS 7 samples from Biache-Saint-Vaast and Montmaurin-La Niche (France) than with later Neanderthals, although the observed traits are also widely shared with Atapuerca-Sima de los Huesos. Importantly, the assemblage exhibits internal variability, with less derived morphology primarily confined to anterior teeth from the lower stratigraphic levels. The Payre dental record documents persistent regional variability within the Neanderthal clade during MIS 7. This variability may reflect localized demographic processes, possibly including small-scale admixture associated with climatic fluctuations during the Middle Pleistocene.

Keywords µCT · Dental morphometrics · Middle Pleistocene hominins · Neanderthals · Europe

Laura Martín-Francés and Marina Martínez de Pinillos contributed equally to the article.

✉ Laura Martín-Francés
lauramartinfrancesmf@gmail.com

1 CENIEH (Centro Nacional de Investigación sobre la Evolución Humana), Paseo de la Sierra de Atapuerca 3, Burgos 09002, Spain

2 Monash Biomedicine Discovery Institute, Department of Anatomy and Developmental Biology, Monash University, Melbourne, VIC 3800, Australia

3 Laboratorio de Evolución Humana (LEH), Universidad de Burgos, Plaza Misael Bañuelos s/n, Burgos 09001, Spain

4 University College London Anthropology, London, UK

5 Laboratorio de Poblaciones del Pasado, Universidad Autónoma de Madrid, Madrid, Spain

6 Univ. Lille, CHU Lille, ULR 7367 - UTML&A - Unité de Taphonomie Médico-Légale & d'Anatomie, Lille F-59000, France

7 Centro Mixto, Universidad Complutense de Madrid - Instituto de Salud Carlos III de Evolución y Comportamiento Humanos, Madrid 28029, Spain

8 Departamento de Paleontología, Facultad de Ciencias Geológicas, Universidad Complutense de Madrid, Madrid 28040, Spain

9 MNHN, UMR 7194, UPVD, 1 rue René Panhard, Paris 75013, France

Published online: 20 May 2026

Introduction

The origin and evolution of the Neanderthal clade remains one of the most intricate topics in the field of human evolution. Recent paleogenetic and paleoanthropological evidence indicates that the roots of the Neanderthals extend as far back as MIS 12, represented by the Atapuerca-Sima de los Huesos population whose hominins show clear morphological and genetic affinities with later Neanderthals (e.g., Arsuaga et al. 2014; Martinón-Torres et al. 2012; Meyer et al. 2016; Meyer et al. 2014). Morphological data further suggests that several European Middle Pleistocene (MP) populations share a common phylogenetic history (e.g., Arsuaga et al. 2014; Daura et al. 2017; Vialet et al. 2018; Zanolli et al. 2018). However, despite this common history, European MP hominins display substantial morphometric variability. This variability has been interpreted as reflecting complex populations interactions resulting in different lineages within the Neanderthal clade (e.g., Bermúdez de Castro et al. 2019; Martínez de Pinillos et al. 2020; Roksandic et al. 2011; Verna et al. 2020; Vialet et al. 2018), rather than a linear evolutionary process (e.g., Hublin 2009). Increasingly, morphometric evidence supports a scenario involving repeated population dispersals, regional fragmentation, and gene-flow within Europe during the Middle and Late Pleistocene (Dennell et al., 2009, 2011; MacDonald et al. 2012). Genomic data further complicate this picture. Neanderthal genome document episodes of gene flow not only among Neanderthals but also between Neanderthals and other hominin groups, including *H. sapiens* and Denisovans, indicating that Neanderthal evolution occurred within a network of interacting populations, which may have influenced patterns of morphological diversity (e.g., Posth et al. 2017; Prüfer et al. 2017; Slon et al. 2018).

Particularly debated are hominins dating to MIS 7 − 5, which have been argued to display a distinctive combination of traits that differentiate them from both earlier (MIS 12 − 8) and later (MIS 4 − 3) Neanderthal populations (e.g., Arsuaga et al. 1997; Couture and Hublin 2005; Dean et al. 1998; Guipert et al. 2011). Yet the limited fossil record from this period in Europe represents a major challenge to understanding the evolution of the Neanderthal clade, from the earliest representatives to the most recent classic Neanderthals. Continued study of new fossil discoveries together with the reassessment of previously studied fossils, is therefore essential to refining our understanding of the variability within the MP hominins and, ultimately, the evolutionary history of the Neanderthal clade.

Fig. 1 Stratigraphic sequence of the Payre site, showing the different units, Marine Isotope Stages (MIS), and the position of the human remains (indicated by black stars).Modified from Valladas et al. (2008).

Background on Payre site

The Payre site is located in the Rhône valley (South-East, France). The cave was transformed into a shelter by erosive processes with cryoclastic events and collapse of the cave roof (Moncel et al. 2002; Moncel 2008). Excavations carried out by M.H. Moncel uncovered archaeological levels (A-I) covering 20 to 50 m^2 and 5 m in thickness. The 16 human remains (twelve teeth, two fragments of parietal bones and two fragmentary mandibles) were discovered in several levels, mainly F and G (Fig. 1). The archaeological sequence extends from MIS 9 to the end of MIS 6 based on ESR-U series, TL and TIMS (Condemi and Moncel 2008; Moncel et al. 2019; Valladas et al. 2008). The average TL ages published by Valladas et al. (2008) for levels G (247±29 ka) and F (251±25 ka) provide a similar chronological time for the occupations (end of MIS 8-beginning of MIS 7), in agreement with ESR/U-series on teeth and bones, ranging from 139±16 ka (D) and 265±59 ka (G) (Richard et al. 2021).

The cave was predominantly occupied by humans, although it also served intermittently as a den for carnivores and *Ursus*. The highest density of bears is for level F (alternating occupation by bears and humans) when the size of the cavity decreased, while level G was more anthropic (less density of bears and carnivores remains). The oldest stratigraphic unit containing archaeological material (unit G, comprising two phases of occupation, layers Ga and Gb) dates to approximatively 250 ka, MIS 7 (Valladas et al. 2008). Most of the human remains, including teeth, mandibular and parietal bones, derive from this unit. Layer Gb yielded three teeth and layer Ga five teeth, two fragments of parietal and two mandibules (Cavillac et al. 2025). The second unit (unit F divided in 4 sublevels, Fa to Fd), provided evidence of less densely distributed occupations and is also dated to MIS 7. This unit yielded three human teeth and one tooth at the top covered by a major collapse of the cave (level E). The unit F was sealed by a major collapsing event, corresponding to the end of MIS 6. The final occupations occurred beneath the rock shelter (Fig. 2).

The faunal assemblage is dominated by herbivores, including *Equus ferus*, *Stephanorhinus kirchbergensis*, *Stephanorhinus hemitoechus*, *Elephas*, *Bos primigenius*, *Hemitragus bonali*, *Cervus elaphus*, *Capreolus capreolus*, *Castor fiber*, *and Ursus spelaeus*, as well as carnivores such as *Panthera leo spelaea*, *Cuon priscus*, *Felis silvestris*, *Lynx lynx*, and *Vulpes vulpes*. Faunal remains indicate consistent patterns of human activity throughout the sequence, with evidence of hunting primarily targeting *Cervus elaphus*

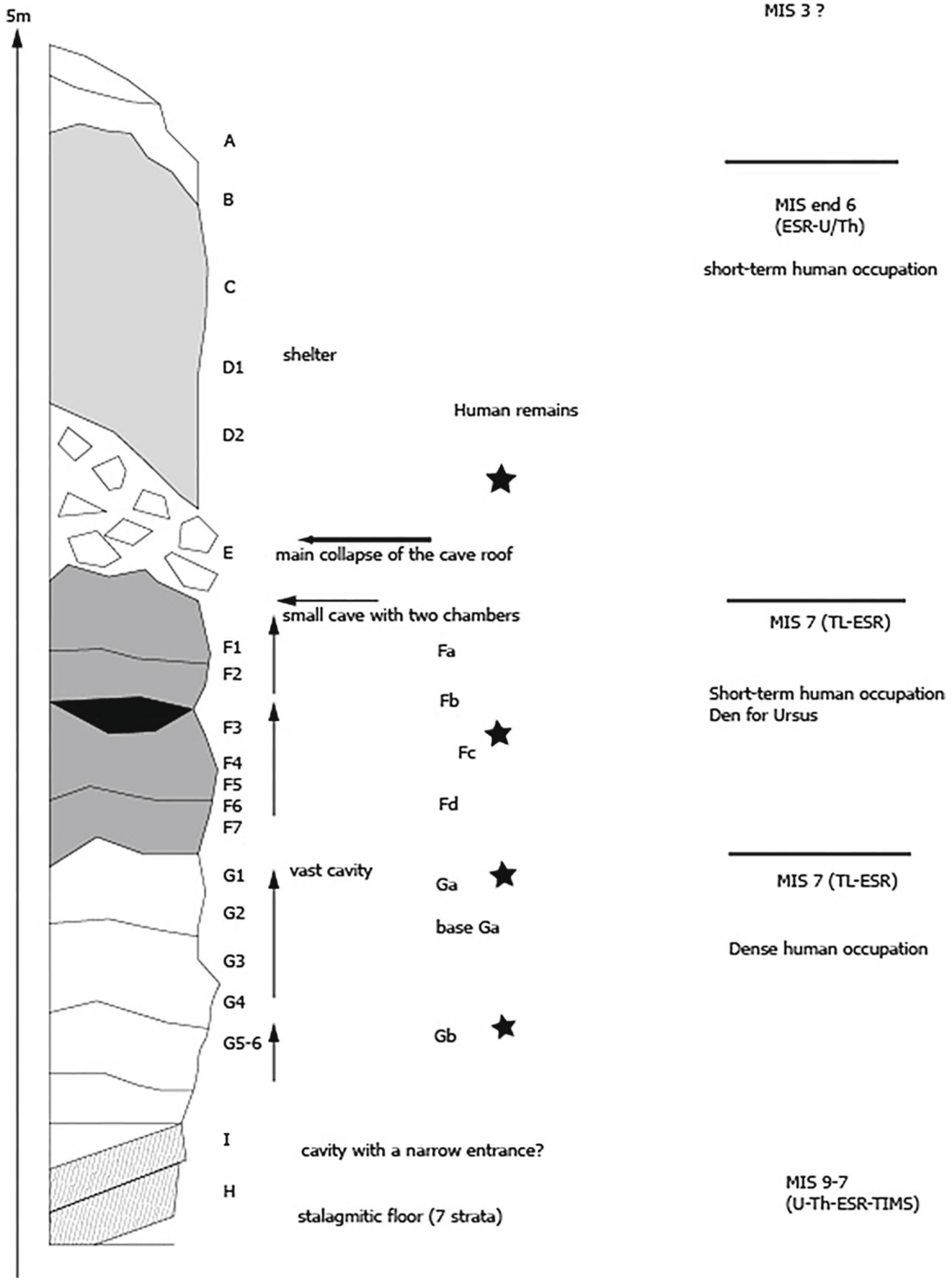
5m
MIS 3 ?
A
B
C
D1
D2
E
shelter
Human remains
main collapse of the cave roof
small cave with two chambers
MIS end 6
(ESR-U/Th)
short-term human occupation
MIS 7 (TL-ESR)
F1
F2
F3
F4
F5
F6
F7
Fa
Fb
Fc
Fd
Short-term human occupation
Den for Ursus
G1
G2
G3
G4
G5-6
vast cavity
Ga
base Ga
Gb
MIS 7 (TL-ESR)
Dense human occupation
I
H
cavity with a narrow entrance?
stalagmitic floor (7 strata)
MIS 9-7
(U-Th-ESR-TIMS)

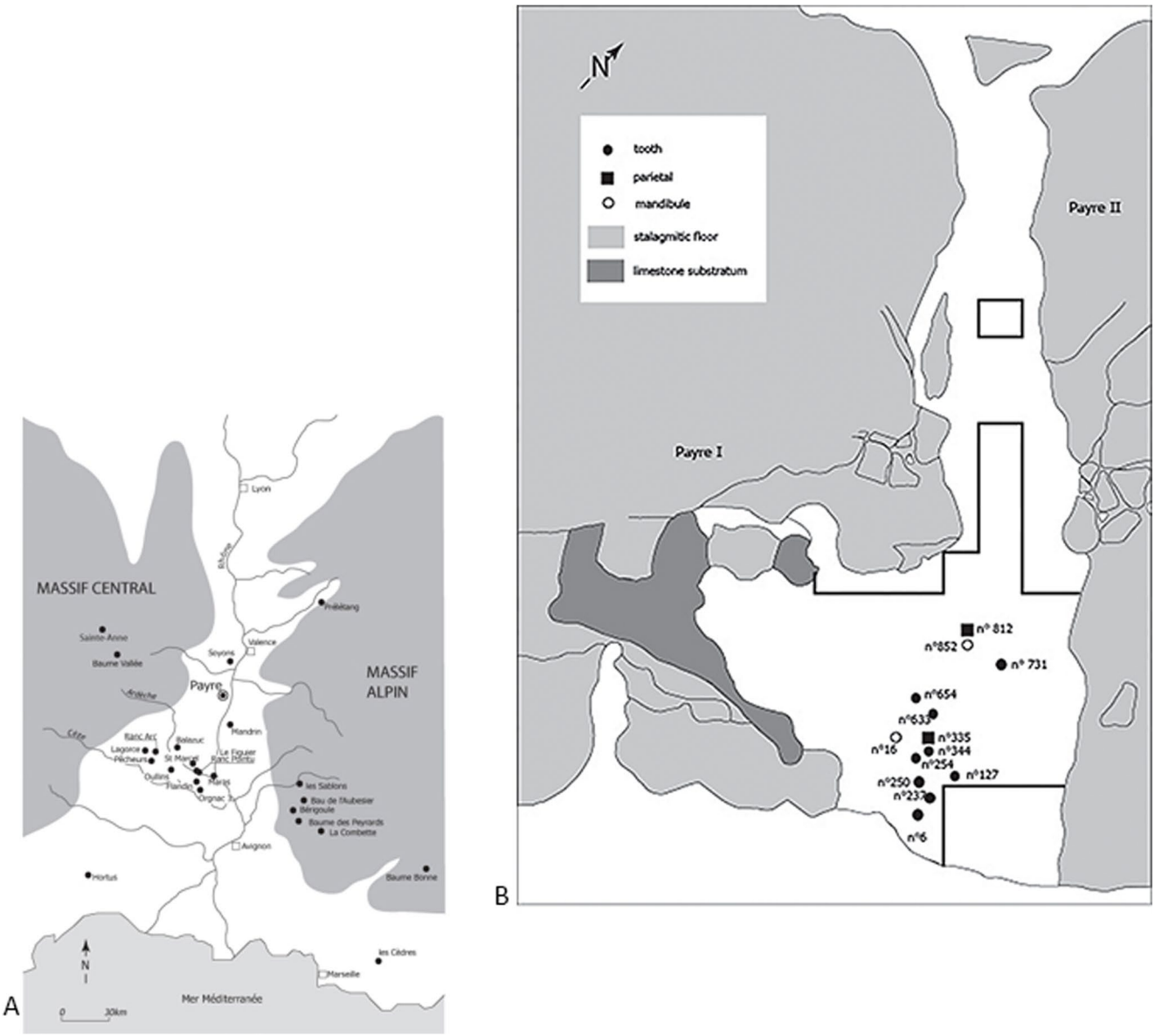

Fig. 2 2 A. Location of the Payre site in France. 2B. Plan view of the site showing the spatial distribution of all human remains. Teeth in this study, include: Payre 9–29 (stratigraphic level E); Payre 14–336, Payre 10–482 and Payre 13–717 (stratigraphic level F); Payre 8–344, Payre 6–127 and Payre 11–633 (stratigraphic level Ga); Payre 3–250 and Payre 2–237 (stratigraphic level Gb). For further details on the dental collection included in this study see Table 1

ssp., *Bos primigenius and Equus cf. mosbachensis*, while rhinoceroses and elephants were likely scavenged. Some bear bones also show signs of human exploitation (Lateur et al. 2024). Zooarchaeological analyses suggest repeated, short-term, seasonal occupations longer for levels G and D than for level F, in agreement with the density of remains of *Ursus* for level F (Rivals et al. 2009). Evidence of fire use was found in all levels, and an ashy lens was identified at the top of Layer Ga, although no clear hearth structure was documented (Moncel 2008). Bone remains were intensively fractured, and some exhibit burning traces, as flint artefacts (Moncel 2008).

The presence of remains of species such as *Bison sp.*, *Capreolus capreolus ssp.*, *Megaloceros sp.*, *Capra ibex*, *Hemitragus sp.*, *Rupicapra sp.* and *Sus scrofa ssp.*. indicates various ecosystems around the site: open in the vicinity of the cave and forested in the valley (Rivals et al. 2009). Isotopic analyses of both human and animal remains indicate a stable subsistence strategy over time and a reliance on local resources for humans, although some evidence of human mobility has been documented for instance through the analyse of lead into child teeth (Bocherens et al. 2016; Ecker et al. 2013; Moncel et al. 2019; Smith et al. 2018). The lithic assemblages are

attributed to the Early Middle Paleolithic (Baena et al. 2017; Carmignani et al. 2017), with flint being the predominant raw material, supplemented by local stones. The core technology is mostly discoidal and orthogonal and the retouched artefacts are scrapers and points. Some large tools (bifaces, bifacial scrapers, simple scrapers) are made on quartzite, limestone and basalt pebbles or large flakes. Micro-wear studies demonstrate the diversity of activities on the site (Hardy and Moncel 2011; Moncel 2008; Pedergnana et al. 2018).

Previous analyses of the morphometric characteristics of the Payre dental remains have identified a combination of traits, encompassing features typical of MIS 12–8 populations alongside traits characteristic of later "classic" Neanderthals (MIS 4–3), thereby underscoring the morphological variability within the Neanderthal clade (e.g., Moncel and Condemi 2007; Moncel 2008). In this context, we present a morphometric reassessment of the Payre dental remains. By incorporating new approaches, including morphometric characterization of the EDJ, dental tissue proportions, and expanded comparative datasets, we aim to identify additional traits that may clarify the affinities of the Payre sample with earlier and later Neanderthal populations or if the dental morphology of the Payre population differentiates them from both earlier and later Neanderthal groups. More broadly, this study seeks to contribute to our understanding of the evolutionary dynamics of the Neanderthal clade within the framework of European population fragmentation and regional differentiation.

Morphologically, the Payre dental remains are expected to align with fossils from the MIS 7 − 5 such as those from Montmaurin-La Niche, Biache Saint-Vaast (BSV), and Krapina. Moreover, based on chronological grounds, we hypothesize that dental remains from lower levels, corresponding to MIS 7 will exhibit greater similarities with earlier Neanderthals, while those from upper levels, corresponding to the end of MIS 6, will display more similarities with later members of the Neanderthal clade.

Material

The sample from the Payre site analysed in this study comprises nine isolated maxillary and mandibular dental remains from 4 archaeological levels (E, F, Ga, Gb). Here we provide both sets of specimen identifiers: Payre 1 to 15, as designated by Verna and colleagues (2020), and their corresponding excavation numbers as reported by Condemi and Moncel (2008). Three specimens, Payre 5, Payre 7, and Payre 15, were excluded from the present study. Payre 5 has been attributed to *H. sapiens* and considered intrusive to the site (Smith et al. 2018); Payre 7 is a left parietal bone fragment and Payre 15 is a mandible described by Verna and colleagues (2020). Two additional human remains were identified more recently: Payre 16, a left part of an edentulous mandible, and Payre 17, a fragment of left parietal (Cavillac et al. 2025).

The specimens considered in this study include: Payre 10–482 (RC'), Payre 13–717 (RP^3), Payre 3–250 (RI_1), Payre 2–237 (RI_2), Payre11-633 (RC,), Payre 8–344 (LP_3), Payre 6–127 (LP_4), Payre 9–29 (RP_3), and Payre 14–336 (LM_2). According to Moncel and Condemi (2007) teeth represent five individuals (see Table 1). Payre 9–29 was initially classified as a P_4 (Moncel and Condemi 2007). However, its rhomboidal contour, globular metaconid, occlusal projection of the buccal cusp and compressed occlusal polygon are more characteristic of a P_3 than a P_4. Consequently, Payre 9–29 has been reclassified as a right P_3.

We did not include the complete sample from Payre in all the analyses due to their preservation and wear degree (Table 1 includes wear scoring following Molnar 1971). The comparative sample in this study consists of 356 teeth from several groups, including the Middle Pleistocene samples from Sima de los Huesos (SH), Arago, Biache-Siant-Vaast (BSV), and Montmaurin-La Niche; Neanderthals from Krapina; fossil *H. sapiens* from Qafzeh, and recent modern humans of African and European origin. Table 2 details the full dental sample used in this study and specifies the specimens included in each analysis (for the complete list of specimens see SI Table 1).

Table 1 Payre teeth included in this study (tooth type, associated individual, stratigraphic level, Marine Isotope stage, wear score) and type of analysis performed (OES morphology by ASUDAS scoring, GM of the EDJ rim, and, tissue proportions and distribution)

Specimen	Tooth	Individual	Stratigraphic level	MIS	Wear (Molnar 1971)	ASUDAS	GM	Enamel thickness & Cartographic maps
Payre 9–29	LP_3	A	E	5	3	x		
Payre 14–336	LM_2	B	F	7	4	x		
Payre 10–482	RC'	C	F	7	4	x		
Payre 13–717	RP^3	C	F	7	2–3	x	x	
Payre 8–344	LP_3	D	Ga	7	2	x	x	x
Payre 6–127	LP_4	D	Ga	7	2	x	x	x
Payre 11–633	RC,	D	Ga	7	3	x		x
Payre 3–250	RI_1	E	Gb	7	4–5	x		
Payre 2–237	RI_2	E	Gb	7	4–5	x		

Table 2 Complete sample (original and comparative) included in this study used for morphometric analyses

Sample	Site	Locality	Chronology	MIS	*N*	EDJ Morphology (*N* total)	GM of the EDJ (*N* total)	Enamel Thickness (*N* total)	Reference
Middle Pleistocene *Homo*	**Payre**	**France**		**7–5**	**9**	**9**	**3**	**3**	**Original data**
	Mauer	Germany		15	1	1			Weber et al., 2016
	Montmaurin-La Niche	France		7	1	1			Martínez de Pinillos et al. 2020
	Biache Saint-Vaast			7	2	2	1		Martín-Francés et al., 2023
	Arago	France		12	12	11	4	4	Martínez de Pinillos 2017 and Original data
	Atapuerca-Sima de los Huesos	Spain		12	86	62	20	41	García-Campos et al. 2019 Martín-Francés et al. 2020, 2023, *submitted* and Original data
	Visogliano	Italy		12	2	2			Zanolli et al. 2018
	Qesem Cave	Israel		15	1	1			Hershkovitz et al., 2016 Weber et al., 2016
	Mala Balanica	Serbia		10–11	1	1			Roksandic et al. 2011 Skinner et al. 2016
Early Neanderthals	Krapina	Croatia	Late Pleistocene	5	40	32	13	14	Original data from NESPOS website
Late Neanderthals	Gibraltar Devil´s Tower	Europe		2–3		1			Martínez de Pinillos et al. 2014 and 2017
	La Quina	France		4–3	1	1	1		Original data from NESPOS website
	Sima de las Palomas	Spain		3	2			2	Bayle et al. 2017
	Regourdou	France		5c	2	1		1	Martínez de Pinillos et al. 2014 and 2017 Bayle et al. 2017
	Engis (Schmerling Caves)	Belgium		3	1		1		Original data from NESPOS website
	Oliveira	Portugal		3	1			1	Willman et al., 2012
Fossil *H. sapiens*	Qafzeh	Israel		5b-5	2	3	3		Original data from ESRF website
Modern *H. sapiens*		Sudan	Holocene	1	55	36	30	27	
		South Africa			28			28	
		Europe			114	44	25	45	Martín-Francés et al., 2024

Methods

Scanning of the samples

We employed high-resolution µCT images for the analysis of the samples. The original sample from Payre was scanned at the Muséum national d'Histoire naturelle, France (AST-RX Platform) using a GE 103 Phoenix v/tome/x_L 450 instrument, with the following parameters: 120 kV and 180 µA, 0.5 mm Cu filter and isometric voxel size of 22 µm. The µCT data from the SH, Arago, BSV sites, as well as the recent modern human sample, are part of the Dental Anthropology Group (GAD) database at CENIEH and has been previously published in various studies (e.g., Martínez de Pinillos et al. 2020; Martín-Francés et al. 2020, 2022, 2025; García-Campos et al. 2019). The remaining fossil samples, including the specimens from Krapina and Qafzeh, were downloaded from ESRF (http://paleo.esrf.eu/) and Nespos (https://nespos.org) websites.

Virtual segmentation

The 3D virtual segmentation of the dental tissues (enamel, dentine and pulp) was performed using Amira (6.3.0, FEI

Inc.) with the semiautomatic, threshold-based segmentation tool. These were employed for the characterization of the enamel-dentine junction (EDJ) morphology, tissue proportions, and enamel thickness topographic distribution.

Morphological characterization of the OES and EDJ

We assessed the morphological variation of the outer enamel surface (OES) and the enamel-dentine junction (EDJ) in the sample using the modified version of the Arizona State University Dental Anthropological System (ASUDAS) of Martinón-Torres et al. (2012) and references therein. The scoring systems of Martínez de Pinillos et al. (2014) and Martinón-Torres et al. (2014) were employed to evaluate the expression of the trigonid and talonid crests. In addition, we followed Martin et al. (2017) for the assessment of cusp tip position relative to the marginal ridge, and Compton and Stringer (2015) for the evaluation of distal occluso-lingual clefts and buccal vertical grooves.

Geometric morphometrics of the EDJ

Geometric morphometrics (GM) analyses of the EDJ were conducted on the virtual surfaces of three specimens from Payre (13–717 RP^3, 86–344 LP_3, 6–127 LP_4). Specimens exhibiting large dentine patches (Molnars' category > 3 for premolars and > 4 for molars) were excluded from the analysis, as reliable reconstruction of the dentine horns is not possible. The comparative sample includes specimens from the Middle Pleistocene assemblages of SH, BSV and Arago, Neanderthals from Krapina and La Quina, fossil *H. sapiens* from Qafzeh and recent modern humans of African and European origin (Table 2). Comparative specimens were mirrored according to the side of the preserved teeth from Payre.

To explore patterns of dental morphology and group affinities, we performed both standard Principal Component Analysis (PCA) and between-group PCA (bgPCA). We used the B-spline module in Amira (v. 6.3.0, FEI Inc.) to place one landmark at each of the dentine horn tips of the main cusps of upper (protocone and paracone) and lower premolars (protoconid and metaconid), along with 49 semilandmarks along the marginal ridge. Geometric morphometric analyses were performed in R (v. 4.4.0; R Core Team, 2024). We conducted the weighted PCA and bgPCA based on the Procrustes and deformation-based shape residuals (Mitteroecker and Bookstein 2011). Allometry was assessed using the coefficient of determination (R^2) of a multiple regression analysis (Bookstein 1991), with centroid size as the independent variable and (bg)PC scores as dependent variables (Mitteroecker et al. 2013).

Tissue proportions

We calculated the dental crown tissue proportions of three specimens from Payre (11–633 LC, 8–344 LP_3, 6–127 LP_4) and compared the results to those of SH, Arago, Neanderthals from various locations, fossil *H. sapiens* from Qafzeh, and recent modern humans of African and European origin (Table 2 and see SI Table 1 for a complete description of the specimens). For canines, we followed the method developed by García-Campos et al. (2018b), based on the approach by Benazzi et al. (2014), which uses the cervical curvature as the key morphological feature to virtually isolate the crown and root. For premolars, we followed the protocol of Olejniczak et al. (2008), which defines the cervical plane by separating the crown from the root at the plane halfway between the most apical continuous enamel ring and the plane containing the last hint of enamel. Finally, following the protocols by Kono (2004) and Olejniczak et al. (2008), we measured in Amira (v. 6.3.0, FEI Inc.): (i) the volume of enamel (Ve in mm^3); (ii) the volume of coronal dentine including the pulp enclosed in the crown (Vcdp in mm^3); (iii) the total volume of the crown, including the enamel, dentine and pulp (Vc in mm^3); (iv) surface of the EDJ (SEDJ in mm^2). Then we calculated: (i) the 3D average enamel thickness (3D AET = Ve/SEDJ in mm); (ii) 3D relative enamel thickness (3D RET = 100*3D AET/(Vcdp1/3), a scale-free measurement), and (iii) the percentage of dentine and pulp in the total crown volume (Vcdp/Vc = 100*Vcdp/Vc in %).

Inclusion criteria

We included the C, in the enamel thickness analysis, despite having a wear score of 3 (according to Molnar's categories, 1971). Traditionally, wear category 3, characterized by the absence of the apex in the incisal border and with exposure of a dentine point (Molnar 1971), is regarded as the upper limit to consider them slightly worn (Buti et al. 2017; Feeney et al. 2010; García-Campos et al. 2018a, b, 2019, 2020; Schwartz and Dean 2005). In establishing wear recording procedures, Molnar (1971) considered the original morphology of the tooth and evaluated the canines and incisors together, separated from the premolars and molars due to their multi-cusped morphology. Wear category 3 in incisors and canines, due to the size of their crests (conical and broader), is typically associated with a wider dentine patch than in the premolars and molars (see Fig. 1 of Molnar 1971). However, despite the larger dentine exposure, when quantifying the loss of enamel in those canines exhibiting wear category 3 and varying degrees of dentine exposure, we estimated that the

maximum enamel volume loss is 5.78% (see SI Table 1). Furthermore, when selecting teeth with wear equivalent to that of Payre specimen, we found that the results are similar to those obtained when using all teeth with a wear score of 3 or lower (SI Fig. 1). Thus, although values should be taken with some caution due to reconstruction limitations, we believe a reasonable balance is achieved between the degree of error and the amount of information gained in the characterization of the Payre teeth.

Statistical analyses

For representation purposes, we computed standard boxplots for the three enamel thickness variables (AET, RET and percentage of dentine and pulp) for the original sample from Payre and the comparative sample, including SH, Arago, Neanderthals and recent modern humans. To analyse the similarities in dental tissue proportions between the Payre specimens and the comparative sample, we performed an adjusted Z-score analysis. The Adjusted Z-score test (Maureille et al. 2001; Scolan et al. 2012) allows the comparison of unbalanced and reduced samples (e.g., one specimen against a group) by using Student's inverse t-distribution. Adjusted Z-scores for AET, RET and percentage of dentine variables were calculated to compare 3D dental tissue proportions and enamel thickness values of the three Payre specimens with the means and standard deviations of the SH, Neanderthal and MH groups. In these Z-scores the −1.0 to +1.0 interval comprises the 95% of the variation in the reference samples.

Enamel thickness topographic distribution

We generated the 3D topographic maps using the surface distance module (SDM) in Amira (6.3.0, FEI Inc.). The distance between the OES and the EDJ are represented using a chromatic scale from thinnest (blue) to thickest (red) (Bayle et al. 2017; Macchiarelli et al. 2013). In addition to the Payre sample, we selected a comparative sample with minimal enamel wear, including specimens from SH, Arago, Neanderthals from Krapina and recent modern humans. For representation purposes, left premolars were mirror-imaged.

Results

Morphological characterization of the OES and EDJ

We describe the degree of expression of key morphological features at the OES and EDJ in the Payre sample, highlighting their similarities with the comparative sample (see Table 3 for the frequency of trait expression in the sample and SI Table 1 for the individual trait scoring of the complete sample). The description of the results is organized by stratigraphic levels, from top (level E) to bottom (level G).

For most features, Payre exhibits great similarities with members of the Neanderthal clade, both in frequency and degree of expression. Overall, there is a good correspondence between the OES and EDJ surfaces. To avoid redundancy, we only specifically refer to EDJ features in cases where they do not correspond with the OES (in SI Table 3, marked with an asterisk) (Fig. 3).

Stratigraphic level E

Payre 9–29 Left P_3 (Fig. 3A) This tooth is characterized by a rhomboidal contour, with a marked projection of the labial surface of the buccal cusp on the occlusal view, and a small globular lingual cusp. This morphology, characterized by the compression and lingual displacement of the occlusal polygon, is more commonly observed in European MP populations and Neanderthals than in modern humans. The tooth has a well-developed distal accessory ridge (grade 1) and a continuous transverse crest (grade 2), traits frequently recorded in SH, Neanderthals, but rarely in modern humans (Martinón-Torres et al. 2012 and this study). No accessory lingual cusps are present; instead, we observe a distolingual platform with a slight ridge elevation (grade 2). This conformation is commonly found in Neanderthals and early Neanderthal groups, in contrast to the absence of lingual cusps and ridges seen in *H. sapiens* (Martinón-Torres et al. 2012). Although the labial surface is smooth, there is a basal bulging typical of SH and most Neanderthal groups.

Stratigraphic level F

Payre 14–336 Left M_2 (Fig. 3B) This molar has five cusps, although the hypoconulid is relatively small (grade 2). The cusps are arranged in a cruciform pattern, a derived feature for the genus *Homo* that is less frequent in Neanderthals than in SH and *H. sapiens*, and tends to be associated with the cusp reduction (Martinón-Torres et al. 2012; Skinner et al. 2016; Scott et al., 2018, and this study). The expression of a short and deep anterior fovea is particularly informative. Moreover, the anterior fovea is pronounced (grade 2) a trait expressed in over 70% in Neanderthals and early Neanderthals (Bailey 2002; Martinón-Torres et al. 2012), but rarely present in this particular shape in early and *H. sapiens*. In addition, Payre 336 exhibits a continuous mid-trigonid crest at both the OES and EDJ (type 10 of Martínez de Pinillos et al. 2014). The

Table 3 Frequencies of the degrees of expression of main morphological traits in the EDJ surfaces of Payer specimens and the comparative samples (SH: Sima de los Huesos, MP: Middle Pleistocene *Homo*, NEA: Neanderthals, FHS: fossil *H. sapiens* and MH: modern humans). See SI Table 1 for the individual scoring of each specimen

I_1	Grade	Payre	SH	MP	NEA	FHS	MH
Labial convexity	**0**	0	0	0			8 (100%)
	1	0	0	0			0
	2	1 (100%)	7 (87.5%)	2 (100%)			0
	3	0	1 (12.5%)	0			0
	4	0	0	0			0
	5	0	0	0			0
	6	0	0	0			0
	Total	1	8	2			8
Shovel shape	**0**	0	0	0			7 (87.5%)
	1	1 (100%)	5 (62.5%)	0			1 (12.5%)
	2	0	3 (37.5%)	2 (100%)			0
	3	0	0	0			0
	4	0	0	0			0
	5	0	0	0			0
	6	0	0	0			0
	Total	1	2	2			8
Tuberculum dentale	**0**	1 (100%)	7 (87.5%)	1 (50%)			7 (87.5%)
	1	0	1 (12.5%)	0			1 (12.5%)
	2	0	0	1 (50%)			0
	3	0	0	0			0
	4	0	0	0			0
	5	0	0	0			0
	6	0	0	0			0
	Total	1	8	2			8
I_2	**Grade**	**Payre**	**SH**	**MP**	**NEA**	**FHS**	**MH**
Labial convexity	**0**	0	0	0			8 (100%)
	1	0	0	0			0
	2	1 (100%)	8 (100%)	0			0
	3	0	0	2 (100%)			0
	4	0	0	0			0
	5	0	0	0			0
	6	0	0	0			0
	Total	1	8	2			8
Shovel shape	**0**	0	0	0			7 (87.5%)
	1	0	1 (12.5%)	0			0
	2	1 (100%)	7 (87.5%)	0			1 (12.5%)
	3	0	0	1 (50%)			0
	4	0	0	1 (50%)			0
	5	0	0	0			0
	6	0	0	0			0
	Total	1	8	2			8
Tuberculum dentale	**0**	1 (100%)	8 (100%)	1 (50%)			8 (100%)
	1	0	0	0			0
	2	0	0	0			0
	3	0	0	0			0
	4	0	0	1 (50%)			0
	5	0	0	0			0
	6	0	0	0			0
	Total	1	8	2			8
C’	**Grade**	**Payre**	**[1]SH**	**[2]MP**	**[1,2]NEA**	**[2]FHS**	**[1]MH**
Shovel shape	**0**	0	0		0		1 (6.66%)
	1	0	0		0		4 (26.66%)
	2	0	0		1 (9.09%)		4 (26.66%)
	3	0	2 (25%)		3 (27.27%)		3 (20%)
	4	0	3 (37.5%)		3 (27.27%)		3 (20%)
	5	0	2 (25%)		3 (27.27%)		0
	6	1 (100%)	1 (12.5%)		1 (9.09%)		0
	Total	1	8		11		15

Table 3 (continued)

I_1	Grade	Payre	SH	MP	NEA	FHS	MH
Tuberculum dentale	**0**	0	0		1 (9.09%)		7 (46.66%)
	1	0	0		0		1 (6.66%)
	2	0	0		1 (9.09%)		5 (33.33%)
	3	0	0		0		0
	4	0	0		2 (18.18%)		2 (13.33%)
	5	0	6 (75%)		3 (27.27%)		0
	6	1 (100%)	2 (25%)		4 (36.36%)		0
	Total	1	8		11		15
Distal Accesory ridge	**0**	1 (100%)	4 (50%)		6 (54.54%)		5 (33.33%)
	1	0	3 (37.5%)		4 (50%)		4 (26.66%)
	2	0	1 (12.5%)		1 (12.5%)		6 (40%)
	Total	1	8		11		15
Mesial Ridge	**0**	1 (100%)	0		8 (72.72%)		14 (93.33%)
	1	0	2 (25%)		1 (12.5%)		0
	2	0	6 (75%)		2 (18.18%)		1 (6.66%)
	Total	1	8		11		15
C,	**Grade**	**Payre**	**SH**	**MP**	**NEA**	**FHS**	**MH**
Shovel shape	**0**	0	0		0		0
	1	0	0		0		9 (60%)
	2	1 (100%)	0		0		1 (6.66%)
	3	0	0		2 (28.57%)		4 (26.66%)
	4	0	6 (75%)		5		1 (6.66%)
	5	0	2 (25%)		5 (71.42%)		0
	6	0	0		0		0
	Total	1	8		7		15
Tuberculum dentale	**0**	1 (100%)	0		7 (100%)		11 (73.33%)
	1	0	6 (75%)		0		2 (13.33%)
	2	0	2 (25%)		0		2 (13.33%)
	3	0	0		0		0
	4	0	0		0		0
	5	0	0		0		0
	6	0	0		0		0
	Total	1	8		7		15
Distal Accesory ridge	**0**	1 (100%)	6 (75%)		1 (14.28%)		10 (66.66%)
	1	0	2 (25%)		1 (14.28%)		2 (13.33%)
	2	0	0		5 (71.42%)		3 (20%)
	Total	1	8		7		15
Mesial Ridge	**0**	1 (100%)	1 (100%)		7 (100%)		14 (93.33%)
	1	0	0		0		1 (6.66%)
	2	0	0		0		0
	Total	1	8		7		7
P^3	**Grade**	**Payre**	**SH**	**MP***	**NEA**	**FHS**	**MH**
Distal Accessory Ridge	**0**	1 (100%)	1 (33.3%)	0	3 (60%)		4 (50%)
	1	0	2 (66.6%)	3 (100%)	2 (40%)		4 (50%)
	Total	1	3	3	5		8
Mesial Accessory Ridge	**0**	1 (100%)	2 (66.7%)	3 (100%)	4 (80%)		5 (62.5%)
	1	0	1 (33.3%)	0	1 (20%)		3 (37.5%)
	Total	1	3	3	5		8
Transverse Crest of Premolars	**0**	0	2 (66.7%)	0	1 (20%)		6 (75%)
	1	0	0	2 (40%)	1 (20%)		2 (25%)
	2	1 (100%)	1 (33.3%)	3 (60%)	3 (60%)		0
	Total	1	3	5	5		8
Buccal Essential Crest or Ridge	**0**	0	0	0	0		0
	1	0	2 (66.7%)	2 (66.7%)	3 (60%)		8 (100%)
	2	1 (100%)	1 (33.3%)	1 (33.3%)	2 (40%)		0
	Total	1	3	3	5		8
Lingual Essential Crest or Ridge	**0**	0	1 (33.3%)	0	0		2 (25%)
	1	0	1 (33.3%)	1 (33.3%)	3 (60%)		6 (75%)
	2	1 (100%)	1 (33.3%)	2 (66.7%)	2 (40%)		0
	Total	1	3	3	5		8
P_3	**Grade**	**Payre**	**SH**	**MP**	**NEA**	**FHS**	**MH**

Table 3 (continued)

I_1	Grade	Payre	SH	MP	NEA	FHS	MH
Distal Accessory Ridge	**0**	1 (50%)	3 (50%)	1 (50%)	0	1 (50%)	2 (14.28%)
	1	1 (50%)	3 (50%)	1 (50%)	3 (100%)	1 (50%)	12 (85.71%)
	Total	2	6	2	3	2	14
Mesial Accessory Ridge	**0**	2 (100%)	5 (83.33%)	2 (100%)	3 (100%)	2 (100%)	8 (57.14%)
	1	0	1 (16.66%)	0	0	0	6 (42.85%)
	Total	2	6	2	3	2	14
Transverse Crest	**0**	0	1 (16.66%)	0	0	0	1 (7.14%)
	1	1 (50%)	1 (16.66%)	0	1 (33.33%)	0	2 (14.28%)
	2	1 (50%)	4 (66.66%)	2 (100%)	2 (66.66%)	2 (100%)	11 (78.57%)
	Total	2	6	2	3	2	14
Lingual cusp variation	**1**	0	1 (16.66%)	0	1 (33.33%)	1 (50%)	3 (21.42%)
	2	2 (100%)	0	1 (50%)	1 (33.33%)	0	0
	3	0	4 (66.66%)	1 (50%)	1 (33.33%)	1 (50%)	9 (64.28%)
	4	0	1 (16.66%)	0	0	0	2 (14.28%)
	Total	2	6	2	3	2	14
P_4	**Grade**	**Payre**	**SH**	**MP**	**NEA**	**FHS**	**MH**
Distal Accessory Ridge	**0**	0	1 (9.09%)	0	3 (42.85%)	0	15 (51.72%)
	1	1 (100%)	10 (90.90%)	1 (100%)	4 (57.14%)	1 (100%)	14 (48.27%)
	Total	1	11	1	7	1	29
Mesial Accessory Ridge	**0**	1 (100%)	11 (100%)	1 (100%)	6 (85.71%)	1 (100%)	21 (72.41%)
	1	1	0	0	1 (14.28%)	0	8 (27.58%)
	Total		11	1	7	1	29
Transverse Crest	**0**	0	0	0	0	0	10 (34.48%)
	1	0	1 (9.09%)	0	1 (14.28%)	0	12 (41.37%)
	2	1 (100%)	10 (90.90%)	1 (100%)	6 (85.71%)	1 (100%)	7 (24.13%)
	Total	2	11	1	7	1	29
Lingual cusp variation	**1**	0	0	0	0	0	8 (27.58%)
	2	0	0	0	0	0	0
	3	1 (100%)	2 (18.18%)	0	1 (14.28%)	1 (100%)	16 (55.17%)
	4	0	9 (81.81%)	1 (100%)	5 (71.42%)	0	5 (17.24%)
	5	1	0	0	1 (14.28%)	0	0
	Total		11	1	7	1	29
M_2	**Grade**	**Payre**	**SH**	**MP**	**NEA**	**FHS**	**MH**
Fovea Anterior	**0**	0	0	1 (11.11%)	0	1 (50%)	25 (73.52%)
	1	0	0	2 (22.22%)	0	1 (50%)	4 (11.76%)
	2	1 (100%)	10 (100%)	6 (66.66%)	9 (100%)	0	5 (14.70%)
	Total	1	10	9	9	2	34
Trigonid Crest	**1**	0	1 (10%)	0	0	0	2 (5.88%)
	2	0	2 (20%)	0	0	0	2 (5.88%)
	3	0	0	0	1 (11.11%)	0	1 (2.94%)
	4	0	0	3 (33.33%)	0	2 (100%)	22 (64.70%)
	5	0	0	0	0	0	0
	6	0	0	0	1 (11.11%)	0	0
	7	0	0	1 (11.11%)	1 (11.11%)	0	1 (2.94%)
	8	0	0	0	0	0	3 (8.82%)
	9	0	0	0	0	0	0
	10	1 (100%)	1 (10%)	2 (22.22%)	2 (22.22%)	0	2 (5.88%)
	11	0	0	0	0	0	0
	12	0	3 (30%)	3 (33.33%)	2 (22.22%)	0	0
	13	0	4 (40%)	0	0	0	0
	14	0	0	0	2 (22.22%)	0	1 (2.94%)
	Total	1	10	9	9	2	34
Talonid Crest	**0**	1 (100%)	10 (100%)	9 (100%)	9 (100%)	2 (100%)	33 (97.14%)
	1	0	0	0	0	0	0
	2	0	0	0	0	0	0
	3	0	0	0	0	0	0
	4	0	0	0	0	0	1 (2.85%)
	5	0	0	0	0	0	0
	6	0	0	0	0	0	0
	Total	1	10	9	9	2	34

Table 3 (continued)

I_1	Grade	Payre	SH	MP	NEA	FHS	MH
Deflective Wrinkle	**0**	1 (100%)	10 (100%)	9 (100%)	9 (100%)	2 (100%)	34 (100%)
	1	0	0	0	0	0	0
	2	0	0	0	0	0	0
	Total	1	10	9	9	2	34
Hypoconulid	**0**	0	3 (30%)	2 (22.22%)	1 (11.11%)	0	22 (64.70%)
	1	0	1 (10%)	0	0	0	1 (2.94%)
	2	1 (100%)	2 (20%)	2 (22.22%)	1 (11.11%)	0	1 (2.94%)
	3	0	3 (30%)	1 (11.11%)	4 (44.44%)	0	5 (14.70%)
	4	0	1 (10%)	3 (33.33%)	3 (33.33%)	1 (50%)	2 (5.88%)
	5	0	0	1 (11.11%)	0	1 (50%)	3 (8.82%)
	Total	1	10	9	9	2	34
C6 (entoconulid)	**0**	1 (100%)	7 (70%)	7 (77.77%)	7 (77.77%)	2 (100%)	33 (97.05%)
	1	0	1 (10%)	1 (11.11%)	1 (11.11%)	0	0
	2	0	2 (20%)	0	0	0	0
	3	0	0	1 (11.11%)	1 (11.11%)	0	1 (2.94%)
	Total	1	10	10	9	2	34
C7 (metaconulid)	**0**	0	2 (60%)	9 (100%)	9 (100%)	2 (100%)	34 (100%)
	1	0	0	0	0	0	0
	2	1 (100%)	0	0	0	0	0
	3	0	8 (60%)	0	0	0	0
	4	0	0	0	0	0	0
	Total	1	10	9	9	2	34
Groove pattern	**1 (Y)**	0	4 (40%)	3 (33.33%)	3 (33.33%)	1 (50%)	7 (20.58%)
	2 (X or +)	1 (100%)	6 (60%)	6 (66.66%)	6 (66.66%)	1 (50%)	27 (79.41%)
	Total	1	10	9	9	2	34
Protostylid	**0**	1 (100%)	10 (100%)	8 (90%)	9 (100%)	2 (100%)	29 (85.29%)
	1	0	0	0	0	0	2 (5.88%)
	2	0	0	0	0	0	0
	3	0	0	0	0	0	1 (2.94%)
	4	0	0	0	0	0	0
	5	0	0	0	0	0	0
	6	0	0	1 (10%)	0	0	2 (5.88%)
	7	0	0	0	0	0	0
	Total	1	10	9	9	2	34

MP*: We only scored the complete set of traits in Arago and BSV specimens. In the rest of specimens due to dental wear, we could only score the transverse crest trait

combination of a deep, fissure-like anterior fovea with a high, continuous mid-trigonid crest is a typical Neanderthal feature, with variable frequencies in Middle Pleistocene specimens. It is present in a 74% of the SH hominins M_2 (Martinón-Torres et al. 2012), Mountmarin-La Niche, and Arago 6 and 10, but absent in Mauer, and Mala Balanica (Bailey 2002; Hanegraef et al. 2018; Martínez de Pinillos 2017; Martínez de Pinillos et al. 2014, 2020; Martinón-Torres et al. 2007). However, the mid-trigonid crest of the Arago M_2s (Hanegraef et al. 2018) is weaker and lower than in the Neanderthal clade and Payre 14–336. Despite the degree of occlusal wear exhibited by Payre 14–336, the centrally positioned wear facet may indicate a central placement of the metaconid cusp and dentine horn, a trait observed in Neanderthals (Martin et al. 2017; Bailey 2004). In contrast, the buccal surface of the molar does not exhibit buccal vertical grooves, a feature described by Compton and Stringer (2015) as frequently occurring in European Middle Pleistocene specimens, including SH and Pontnewydd, and in Neanderthals. The concomitant expression of both features (a short, deep or pit-like anterior fovea and a continuous mid-trigonid crest) is virtually absent in *H. sapiens*.

Payre 10–482 Right C′, (Fig. 3C) This tooth is robust and exhibits mass-additive features, typical of the Neanderthal clade, in contrast to the more simplified morphologies found in the *H. sapiens* clade. Payre 10–482 exhibits a grade 6 (Martinón-Torres et al. 2012) of both shovel shape and tuberculum dentale, with the tuberculum dentale taking the shape of an independent cusp, delimited by short grooves from the mesial and distal marginal ridges, with a free apex. This conformation contrasts with the simplified, incisor-like morphologies found in contemporary modern humans (Martinón-Torres et al. 2012 and this study). However, within the Middle Pleistocene specimens, there is a substantial variation in the expression of the tuberculum dentale, being moderate in Mountmarin and faint in Arago (Martinón-Torres et al. 2012 and this study). No distal accessory ridge or mesial

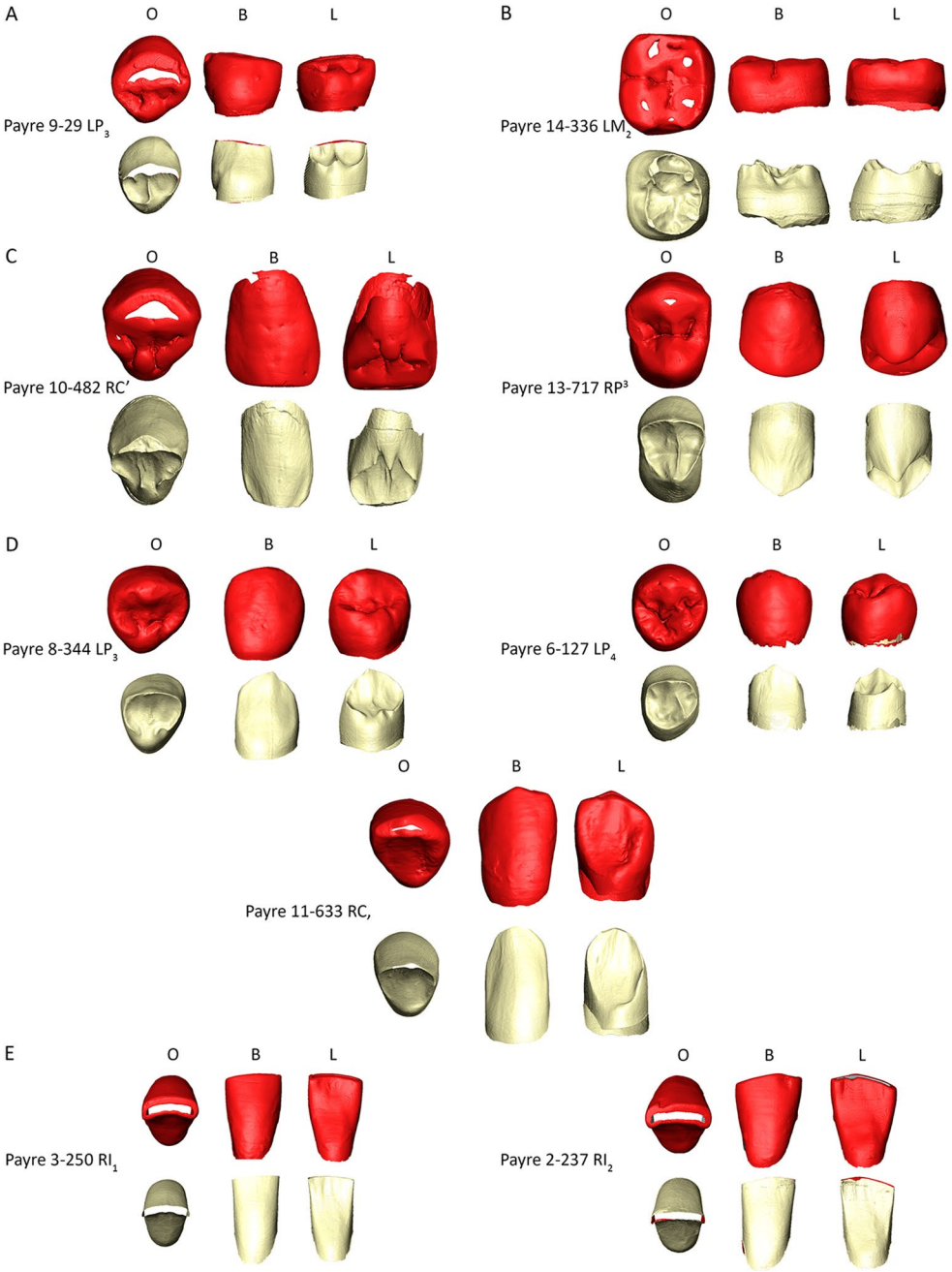

Fig. 3 Payre dental remains organized according to the individuals. 3A. Level E, Payre 9–29 LP_4 (; B. Level F, Payre 14–336 LM_2; C. Level F, Payre 10–482 RC' and Payre 13–717 RP^3; D. Level Ga Payre 8–344 LP_3, Payre 6–127 LP_4 and Payre 11–633 RC, E. Level Gb, Payre 3–250 RI_1 and Payre 2–237 RI_2 (A, B, C, D and E = refers to the individuals' naming; O= occlusal, B= buccal, L= lingual)

canine ridge are present. The mass-additive character of this tooth is further evinced by the presence of several ridges at the EDJ surface, including a continuous crest between the buccal and the lingual cusps.

Payre 13–717 Right P^3 (Fig. 3C) In this tooth, the buccal cusp is larger than the lingual cusp with the buccal and lingual cusps positioned opposite one another. Both main cusps present bifurcated essential ridges (grade 2) a conformation more commonly observed in Neanderthals (with the exception of Krapina D112 and Hortus IX) than in *H. sapiens*. This pattern shows greater variability within Middle Pleistocene groups. The bifurcated buccal crest is present in Arago (Bermúdez de Castro et al. 2019), Wezmeh (Zanolli et al. 2019), BSV (Martín-Francés et al. 2022) and Visogliano (Zanolli et al. 2018) but is absent in Mountmaurin and rare in SH (23.5%, Martinón-Torres et al. 2012). The expression of a continuous transverse crest at the EDJ (grade 2) is a rare trait, observed in the Middle Pleistocene hominin from BSV (Martín-Francés et al. 2022), Visogliano (Zanolli et al. 2018) and one SH individual (Martinón-Torres et al. 2012 and this study). Interrupted thin crests connecting both cusps are more common, though still relatively rare, occurring in 5% of

individuals in the SH population and 6.7% in Neanderthals (Martinón-Torres et al. 2012).

Stratigraphic level Ga

Payre 8–344 Left P^3 (Fig. 3D) This tooth exhibits a rhomboidal contour with a slightly mesially displaced metaconid tip. The buccal surface of the buccal cusp is less projected in the occlusal view compared to Payre 9–29, and the lingual cusp is not expressed as a globular, independent cuspule but rather as a small ridge attached to the mesial marginal ridge. This pattern is predominantly observed in SH and MP groups, 52.9% and 40%, respectively (Martinón-Torres et al. 201 and this study). However, this trait shows significant variability across groups. While some Neanderthals, such as Krapina D111 (this study), display the same pattern as Payre 8–344, Neanderthals also show the highest proportion of specimens with two or even three additional lingual cusps. Moreover, the tooth exhibits a distal occluso-lingual groove cleft, a trait observed in Middle Pleistocene hominins, among others SH and Pontnewydd (Compton and Stringer 2015). Unlike Payre 9–29, specimen Payre 8–344 lacks a transverse crest, features a smooth and flat labial surface, and does not exhibit basal bulging.

Payre 6–127 Left P_4 (Fig. 3D) This tooth displays a round, asymmetrical contour, with a distolingual bulge due to the expression of a talonid. The lingual cup is mesially displaced relative to the buccal cusp tip, a feature commonly found in the Neanderthal clade when compared to *H. sapiens*. Both mesial accessory and distal accessory ridges are present, visible at both the OES and the EDJ. While the mesial accessory ridge is consistently present in all groups, except for SH, the distal accessory ridge is remarkably more frequent in all samples, except for contemporary modern humans (Martinón-Torres et al. 2012). The two main cusps are connected by a continuous transverse crest (grade 2), a feature expressed in high percentages within the Neanderthal clade (75% in SH, 69% in Neanderthals; Martinón-Torres et al. 2012 and this study) and showing more variable frequencies across Middle Pleistocene groups (present in Arago 28 but absent in Mauer and Pontnewydd 5). Payre 6–127 also displays a distolingual talonid, with up to three accessory cusps in the OES and two at the EDJ. The presence of two (grade 4) or more (grades 5) accessory lingual cusps is commonly recorded in MP hominins from SH and Arago as well as Neanderthals (Martinón-Torres et al. 2012 and this study), in contrast to the simplified occlusal surfaces found in *H. sapiens*. Overall, Payre 6–127 shows a conformation that is typically found in *H. neanderthalensis* and most of the European Middle Pleistocene populations (Bailey 2002; Bailey and Lynch 2005; Martinón-Torres et al. 2006), characterized by an asymmetrical contour, a talonid is restricted to the distolingual aspect (with the absence of the distobuccal portion), the presence of more than one accessory distolingual cusp, mesial displacement of the metaconid and a continuous transverse crest.

Payre 11–633 Right C, (Fig. 3D) The morphology of Payre 11–633 is relatively simple, lacking the typically mass-additive features characteristic of Neanderthal populations, except for a pronounced distal marginal ridge (grade 3) versus a faint mesial one (grade 1), conforming an asymmetrical shovel shape. While shovel shape grades 3 and 4 are more frequent in Neanderthals and MP populations (60% and 80%, respectively, with a 74% for SH), grade 1 are rare outside early and contemporary *H. sapiens* (23.5% and 31% versus 5.3% in SH, and 12% in Neanderthals). Neither a distal accessory ridge nor a mesial canine ridge is present. Both the labial and lingual surfaces are smooth, and despite a small basal bulge in the cingular region, no tuberculum dentale is expressed. Apart from the moderate shovel shape in the distal marginal ride, the lack of mass-additive features and simplified aspect is more common in modern humans than in fossil hominin samples.

Stratigraphic level Gb

Payre 3–250 Right I_1 (Fig. 3E) This tooth shows a weak labial convexity (grade 2), which is the predominant pattern in SH but also present in variable frequencies in the rest of the analysed groups. The shovel shape is faint (grade 1), a feature observed in similar percentages in SH, Neanderthals and modern humans, although the absence of shovel shape is more prevalent across all groups (Martinón-Torres et al. 2012 and this study). Similarly, the tuberculum dentale is absent, consistent with the majority of the SH, Neanderthal and modern human samples (Martinón-Torres et al. 2012 and this study). Overall, this dental class is not taxonomically discriminative. Except for a few cases where the Neanderthal clade can show moderately pronounced degrees of tuberculum dentale (grades 2 and 3), there are no morphologically distinctive features among groups.

Payre 2–237 Right I_2 (Fig. 3E) The labial convexity is weak (grade 2), although this feature never exceeds grade 3 in either the Neanderthal clade or *H. sapiens*. The tooth lacks a tuberculum dentale, and most specimens show a smooth lingual surface or a basal eminence that is continuous with the essential ridge, as observed in Payre 237. The shovel shape is faint at the OES, but at the EDJ level, the elevation of the marginal ridges become noticeable (grade 2). The SH shows the highest degree of light shovelling (63.2% presents grade 2), whereas *H. sapiens* exhibit the highest proportion

of non-shovelled I_2s (Martinón-Torres et al. 2012 and this study). Among other MP specimens, light shovelling is present in Arago but absent in Mauer (Martinón-Torres et al. 2012 and this study).

Geometric Morphometrics

Overall, the results are largely consistent between the PCA (SI Figs. 1, 2 and3) and the bgPCA (Figs. 4, 5 and 6), with only minor differences in the position of the specimen Payre 6–127 (left P4). In both analyses, Payre 6–127 occupies the negative end of PC1, within the region of morphospace where teeth with more asymmetrical contours cluster (SI Figs. 3 and 6). However, in the PCA this specimen falls within the area of overlap between Neanderthals and modern humans (SI Fig. 3), whereas in the bgPCA it plots just outside the Neanderthal cluster (Fig. 6). This discrepancy likely reflects the different analytical objectives of the two methods: PCA captures total variance within the sample, while bgPCA maximizes between-group separation, particularly informative for assessing relative group affinities. The broad agreement between the two approaches supports the robustness of the observed morphological patterns in the Payre sample (Figs. 4, 5 and 6; SI Figs. 1, 2 and 3). Given that the primary aim of this study is to evaluate the affinities of the Payre fossils within the Neanderthal clade, we focus here on the bgPCA results, while the PCA plots (SI Figs. 1, 2 and 3) are provided in the Supporting Information.

Stratigraphic level F

Payre 13–717 Right P^3 The bgPC shows a clear differentiation between *H. sapiens* and the other groups along the PC1 (accounting for the 71.57% of the variation). All Neanderthals and Middle Pleistocene specimens (BSV and SH), except for Arago, together with Payre specimen fall in the negative range of the axis, while modern humans cluster towards the positive end (Fig. 4). These specimens

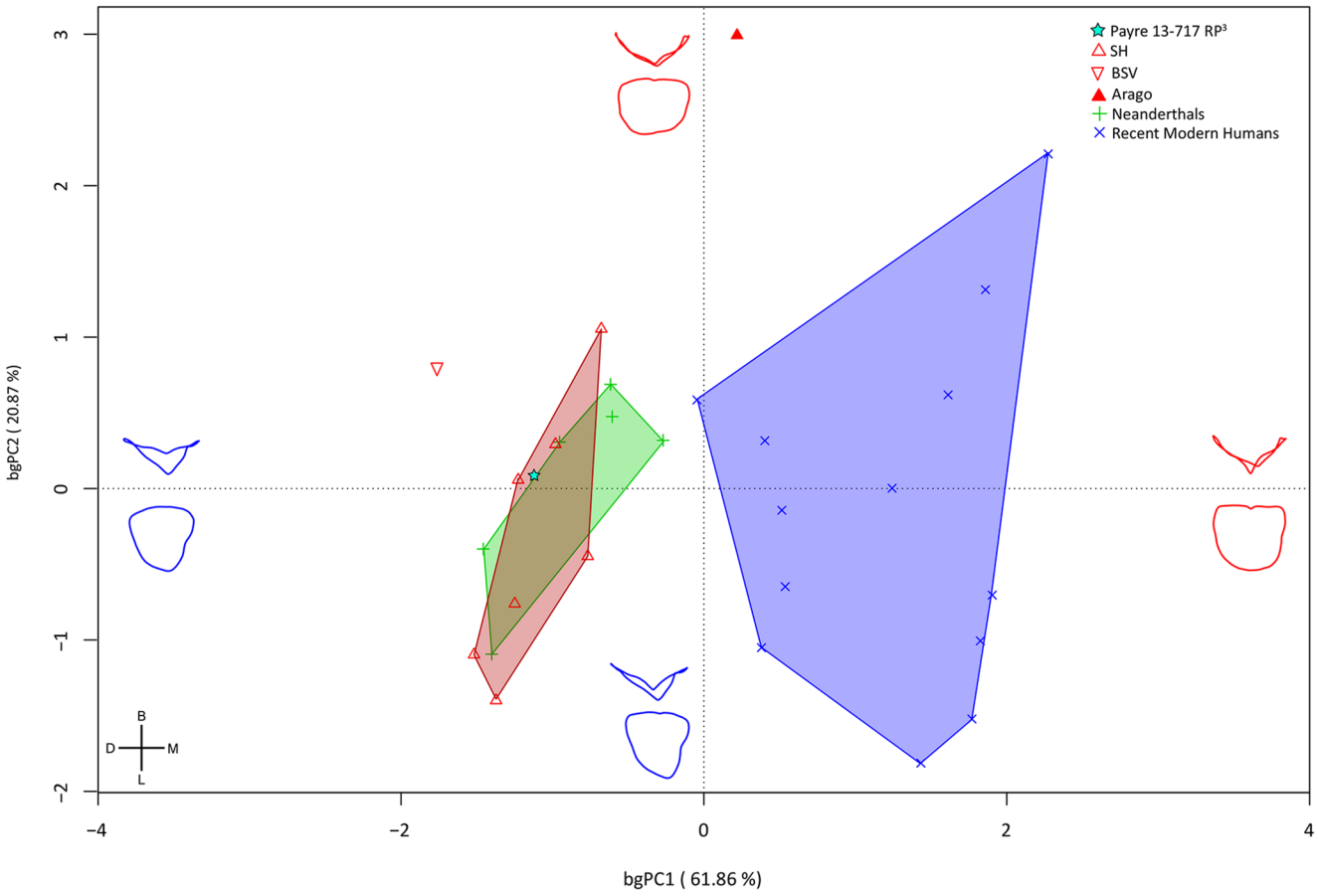

Fig. 4 Between-group principal component analysis (bgPCA) of the Procrustes shape coordinates of the Payre 13–717 RP^3 EDJ compared with those of those of Biache- Saint-Vaast (BSV), Sima de los Huesos (SH), Arago (A), Neanderthals (NEA) and modern humans (MH). The bgPC1 and bgPC2 wireframes, which schematically represent the 3D EDJ, illustrate the maximum morphological variation along each axis. Figure 5. Between-group principal component analysis (bgPCA) of the Procrustes shape coordinates of the Payre 8–344 LP_3 EDJ compared with those of Sima de los Huesos (SH), Arago (A), Neanderthals (NEA) and modern humans (MH). The bgPC1 and bgPC2 wireframes, which schematically represent the 3D EDJ, illustrate the maximum morphological variation along each axis

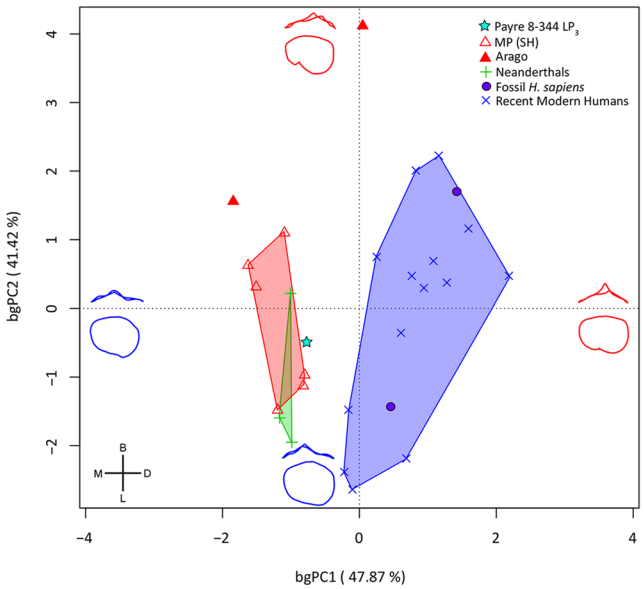

Fig. 5 Between-group principal component analysis (bgPCA) of the Procrustes shape coordinates of the Payre 8–344 LP3 EDJ compared with those of Sima de los Huesos (SH), Arago (A), Neanderthals (NEA) and modern humans (MH). The bgPC1 and bgPC2 wireframes, which schematically represent the 3D EDJ, illustrate the maximum morphological variation along each axis

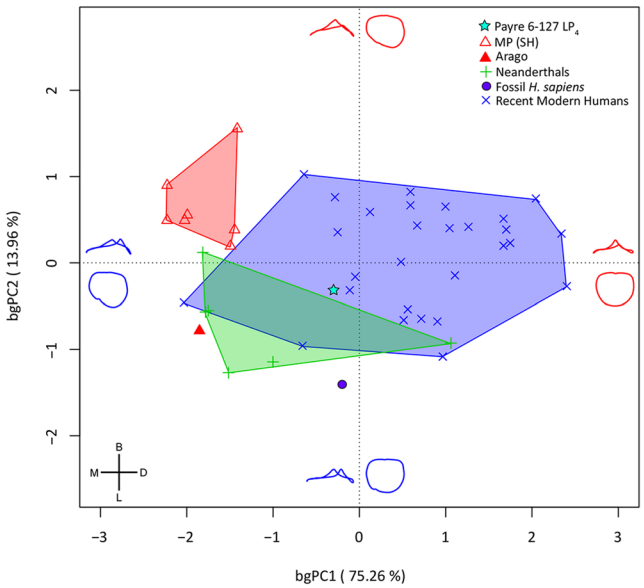

Fig. 6 Between-group principal component analysis (bgPCA) of the Procrustes shape coordinates of the Payre 6–127 LP_4 EDJ compared with those of Sima de los Huesos (SH), Arago (A), Neanderthals (NEA), fossil *H. sapiens* (FHS) and modern humans (MH). The bgPC1 and bgPC2 wireframes, which schematically represent the 3D EDJ, illustrate the maximum morphological variation along each axis

(including BSV, SH, and Neanderthals, the latter two largely overlapping) are characterised by a pentagonal outline of the occlusal rim, where the lingual cusp is comparatively narrower than the buccal one, and the bucco-lingual diameter is larger than the mesio-distal one. In these groups, there is also a marked difference in cusp height and the lingual cusps is mesially displaced relative to the tooth contour. In comparison, *H. sapiens*, on the positive axis of the PC1, display a more quadrangular-shaped EDJ rim. The variation along the PC2 is not discriminative but is noteworthy the position of the Arago specimen at the positive end, characterized by a more quadrangular (mesio-lingually expanded) shape.

Stratigraphic level Ga

Payre 8–344 Left P_3 The bgPCA shows a clear separation between the shape of the EDJ rim of extinct groups and the majority of *H. sapiens* specimens along the PC1 (accounting for the 47.87% of the variation). The Payre specimen falls within the negative PC1 morphospace, closely aligning with the distribution of SH and Neanderthal specimens (Fig. 5). It exhibits a smooth, oval shape with a distolingual protrusion of the lingual cusp. This contrasts with the mesiodistally more expanded EDJ rim of modern humans, where the tips of the cusps tend to protrude inwards towards the center of the tooth. The two Arago specimens show very disparate conformations and while A75 is closer to the Neanderthal clade distribution, A71 falls in the positive extreme of the PC2 variation, with a distolingually protruding contour and strong inward and mesial displacement of the lingual cusp.

Payre 6–127 Left P_4 The bgPCA shows a general separation between Middle Pleistocene groups and *H. sapiens* along the PC1, accounting for the 75.26% of the variation, although there is a considerable overlap between Neanderthals and modern humans. (Fig. 8). Modern humans exhibit the greatest morphological variability of all groups, with specimens spanning both ends of the PC1. While Payre 6–127 falls within the *H. sapiens* group, it is positioned on the negative axis of the PC1, alongside other fossils (SH, Arago, all Neanderthals but one Krapina specimen) and 7 out 21 modern human specimens are located. These are generally characterized by a an asymmetrical EDJ rim, with mesial displacement of the metaconid and the distolingual protrusion of the contour. The metaconid dentine horn is mesially positioned on the lingual EDJ rim (not aligned with the protoconid) and it protrudes towards the occlusal basin, resulting in a bulging lingual rim.

To assess potential allometric effects, we performed Pearson's correlations between shape and size. The results for Payre 13–717 RP^3 ($r^2 = 0.23$, $p = 0.0083$), Payre 8–344 LP^3 ($r^2 = 0.19$, $p = 0.0019$), and Payre 6–127 LP^4 ($r^2 = 0.06$, $p = 0.0903$) indicate no significant allometric influence on PC1. Therefore, shape variation along PC1 is not primarily driven by size.

3D Enamel Thickness

In the Payre sample we observed an increase of the enamel thickness values (AET and RET) in distal direction within the dental series (Table 4; Fig. 7). The AET and RET values for the C, (Payre 11–633) are low (0.73 mm and 13.20 respectively), resembling the Neanderthal mean values and outside the 95% confidence interval of *H. sapiens* (3D AET = 0.72–0.80 mm; 3D RET = 16.90–18.52.90.52, see Fig. 1). The calculated values of enamel thickness in the P_3 (Payre 8–344) (3D AET = 0.96 mm; 3D RET = 17.81) are intermediate between the low Neanderthal and the high RMH mean values, and closer to the Arago and SH mean values (Table 4). Finally, the AET and RET values of the P_4 (Payre 6–127) from Payre are high (3D AET = 1.18 mm; 3D RET = 24.04) close to the mean values of the RMH sample and the Arago specimen, within the range of variation of SH sample but outside of the variation range of the Neanderthal group (Table 4; Fig. 5).

These results are corroborated by the Z-score analysis (Fig. 8). When comparing the values obtained for Payre 11–633 (C,) with the mean and standard deviation of each population, Payre is closer to Neanderthals and then SH than to RMH. The specimen Payre 8–344 (P_3) is within the 95% interval of confidence of Neanderthals and RMH for the three enamel thickness variables. On the contrary, the specimen Payre 6–127 (P_4) only falls within the 95% interval of confidence of RMH for the three enamel thickness variables.

Enamel thickness topographic distribution

Figures 9, 10 and 11 illustrate the pattern of enamel distribution in the Payre specimens and comparative sample. Overall, the cartographic maps corroborate the 3D AET and RET findings.

The distribution pattern of enamel thickness in Payre 11–633 closely resembles that observed in Krapina and SH and different from that of RMH. In Payre 11–633, SH, and Krapina, the enamel cap is thicker on the distal aspect than on the mesial one, particularly at the level of the distal marginal ridge (Fig. 7). In contrast, the lower canines of RMH show thicker enamel that extends along the buccal surface on the incisal half from the distal surface up to the marginal ridge on the incisal half.

In the P_3, we observed differences between the fossil samples and RMH (Fig. 10). Although the thicker enamel (represented by the red colour) is concentrated on the buccal aspect of the crown across species, only RMH also have thicker enamel on the mesial surface. Payre 8–344 and Arago have thinner enamel on the occlusal surface compared to SH and NEA specimens.

In the P_4 (Fig. 11), Payre 6–127, show similar enamel thickness distribution to SH, Arago and RMH specimens. These teeth show thicker enamel concentrated on the buccal and lingual surfaces as well as at the rim and the occlusal surfaces. On the contrary, the Neanderthal specimen from Krapina exhibits the thicker enamel on the buccal surface and some scattered red areas on the occlusal ridges.

Morphometric comparison across stratigraphic levels

The younger Payre 9–29 (a P_3 from level E, MIS 5–6) exhibits a morphological configuration more commonly seen in the SH hominins, e.g., basal eminence and a continuous transverse crest, compared to classic Neanderthals (Martinón-Torres et al. 2012 and this study). The teeth from level F (MIS 7), Payre 14–336 (M_2), Payre 10–482 (C') and Payre 13–717 (P^3), exhibit a suit of morphometric traits that align these specimens particularly with the SH and BSV groups. Notably, the combination of a deep, fissure-like, anterior fovea combined with a high continuous mid-trigonid crest seen in Payre 14–336 (M_2) is widely recorded in SH population but also present in Montmaurin-La Niche and two Arago specimens (Martinón-Torres et al. 2007; Martínez de Pinillos et al. 2014, 2017, 2020; Hanegraef et al. 2018). Additionally, the combination of continuous transverse crest and bifurcated buccal and lingual essential crest observed in Payre 13–717(P^3) is only shared with the specimen 3 from BSV (Martín-Francés et al. 2022). Furthermore, the EDJ rim conformation of Payre 13–717 (P^3) is within the variability of SH. The teeth from level Ga (MIS 7), specimens Payre 8–344 (P_3), Payre 6–127 (P_4), and Payre 11–633 (C,) mostly exhibit morphometric traits aligning them with the Neanderthal clade. Although Payre 8–344 (P_3) does not exhibit the typical suite of Neanderthal morphological traits in its crown, such as a continuous transverse crest or basal bulging in the lingual surface, the morphology of the EDJ rim and the enamel thickness value aligns this specimen with the SH group. Similarly, despite the simpler morphology of Payre 11–633 (C,), which lacks traits such as tuberculum dentale and distal accessory ridge, this tooth is characterized by relatively thin enamel, a condition shared with Neanderthals (Buti et al. 2017), including the early group from SH (García-Campos et al. 2019). Moreover, the MD and BL diameters as well as the robusticity index are within the Neanderthal variability and outside the range of *H. sapiens* (Condemi and Moncel 2008). While the suite of morphological traits of Payre 6–127 (P_4), such as the continuous transverse crest and presence of a talonid, align this specimen with MP groups, such as Arago and SH, as well as later Neanderthals, this tooth is characterized by relatively thick enamel, a condition shared with

Table 4 3D enamel thickness variables assessed in Payre teeth and compared with extinct and extant populations (SH: Sima de los Huesos, A: Arago, NEA: Neanderthals, RMH: Recent Modern Humans)

Sample	Tooth Class	*N*		Ve (mm^3)	Vcdp (mm^3)	SEDJ (mm^2)	3D AET (mm)	3D RET	Vcdp/Vc (%)
	C,								
Payre 11–633		1		119.247	171.635	162.56	0.73	13.20	59.01
SH		12	Mean	107.15	137.42	140.46	0.76	14.88	56.11
			SD	14.47	21.85	16.91	0.06	1.50	2.40
			Range	86.12–133.11	104.22–184.23	118.08–177.94	0.66–0.87	12.79–17.19	53.03–60.22
			95% IC	86.12–133.11	123.54–151.30	129.72–151.21.72.21	0.72–0.80	13–92-15.83	54.59–57.64
A		1		166.55	196.98	181.83	0.92	16.17	54.19
NEA		4	Mean	139.77	213.66	179.38	0.78	13.06	60.38
			SD	21.35	213.66	22.16	0.04	0.65	1.39
			Range	110.36- 159.25	166.65–249.88	149.86–197.97	0.74–0.82	12.10- 13.54	59.12–62.36
			95% IC	105.79–173.79-74	153.63–273.69.63.69	144.12–214.64.12.64	0.72–0.83	12.02–14.09	58.16–62.16-59
RMH		56	Mean	106.35	122.95	121.55	0.87	17.71	53.60
			SD	27.44	31.034	19.78	0.15	3.01	4.35
			Range	63.40- 200.53	72.14- 215.04	93.51 173.11	0.58–1.19	11.09–24.11	46.58–64.01
			95% IC	98.99–113.69.99.69	114.64–131.25.64.25	116.25–126.85.25.85	0.83–0.91	16.91–18.52	52.44–54.76
	P_3								
Payre 8–344		**1**		**127.96**	**157.71**	**133.01**	**0.96**	**17.81**	**55.21**
SH		12	Mean	114.87	121.78	117.36	0.98	19.78	51.40
			SD	13.94	17.35	11.08	0.05	1.05	1.35
			Range	90.27–144.79.27.79	90.78–150.64.78.64	98.35–142.87.35.87	0.87–1.05	17.93–21.33	49.55–54.02
A		2	Mean	132.65	164.63	145.42	0.92	16.87	55.30
			SD	12.99	21.60	12.26	0.17	3.79	5.66
			Range	123.46–141.83.46.83	149.36–179.90	136.75–154.09.75.09	0.80–1.04	14.19–19.55	51.29–59.30
NEA		8	Mean	115.56	148.43	137.74	0.84	15.87	56.97
			SD	24.28	34.97	24.08	0.10	2.45	3.13
			Range	86.01–158.40	99.18–208.00	98.45–168.52.45.52	0.70–0.94	12.81–20.41	51.61–61.11
RMH		23	Mean	102.71	99.12	100.85	1.01	21.91	49.23
			SD	24.20	21.77	14.64	0.13	2.27	2.80
			Range	64.37–143.88.37.88	65.04–138.00	76.94–127.73.94.73	0.76–1.18	17.10–25.96.10.96	44.50–55.54.50.54
	P_4								
Payre 6–127		**1**		**124.594**	**119.59**	**105.19**	**1.18**	**24.04**	**48.98**
SH		17	Mean	122.88	112.40	235.28	1.10	22.96	47.63
			SD	17.05	19.65	36.14	0.06	1.32	1.59
			Range	86.95–147.87.95.87	73.60–140.44.60.44	160.55–283.28.55.28	1.00–1.22.00.22	20.73–25.12	45.38–50.33
A		1		190.71	168.71	146.14	1.30	23.62	46.94
NEA		6	Mean	141.32	173.36	153.05	0.93	16.68	54.99
			SD	13.53	21.78	11.25	0.08	2.06	4.35
			Range	122.02–159.77.02.77	139.88–197.89.88.89	139.56–166.04.56.04	0.81–1.03	13.83–19.92	46.68–59.66
RMH		20	Mean	121.68	102.95	103.18	1.17	24.94	46.17
			SD	29.90	18.52	14.74	0.15	2.61	2.82
			Range	77.90–175.02.90.02	70.36–144.60	77.99–132.34.99.34	0.92–1.50	20.22–31.83	40.84–51.80

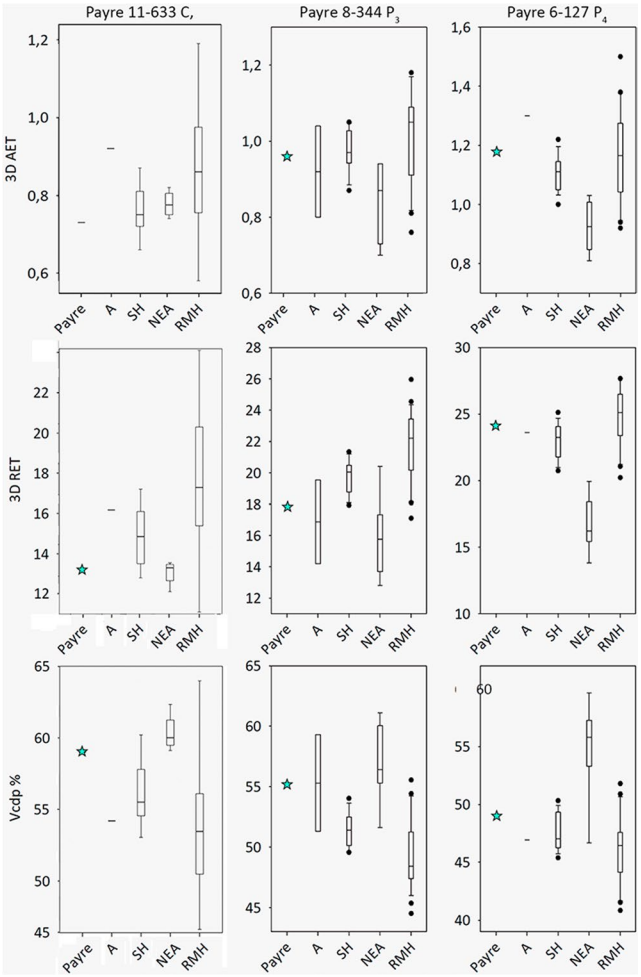

Fig. 7 Box plots of the 3D crown values. 3D values depicting the average enamel thickness (3D AET), relative enamel thickness (3DLRET) and the percentage of dentine and pulp in the crown (Vcdp/Vc) of Payre 14–633 (C,), Payre 8–344 (LP3) and Payre 6–127 (LP4) and the comparative sample

the SH and Arago groups, but not with other Neanderthal groups. In contrast, the configuration of the EDJ rim in Payre 6–127 is closer to the Neanderthal morphology than to the SH and Arago. Finally, the older teeth from level Gb (MIS 7) Payre 3–250 and Payre 2–237, two lower incisors, are characterized by a simple morphology that lacks Neanderthal-like traits, such as basal eminence, observed in early populations from the SH and Visogliano sites as well as some classic Neanderthals (Martinón-Torres et al. 2012; Zanolli et al. 2018). Although this dental class is not taxonomically discriminative due to the absence of morphologically distinctive features among groups, the metrics of these two specimens from Payre do not fall within the ranges of the Neanderthal clade. According to Condemi and Moncel (2008), the two lower incisors are small in size compared to the different groups of the Neanderthal clade, including SH sample, with MD and BL diameters, as well as the robusticity index falling only within the *H. sapiens* range.

Discussion

The scarcity of fossil remains during the MIS 7−5 in Europe complicates interpretations of Neanderthal evolution between earlier MP populations (e.g., SH, Arago, Visogliano) and the emergence of the classic Neanderthals in the Late Pleistocene. Different evolutionary models have been proposed to explain this transition. The organismic model (Rosas et al. 2006) suggests two distinct and successive phases in Neanderthal evolution involving organismic integration processes, whereas the accretion model (Dean et al. 1998; Hublin and Roebroeks 2009), proposes a gradual accumulation of Neanderthal traits through time. Although both frameworks accommodate the chronological pattern of the lineage, they imply different taxonomic interpretations. In this scenario, some authors (e.g., Couture and Hublin 2005; Guipert et al. 2011) have suggested that hominins from MIS 7−5 display a unique combination of traits that differentiates them from both earlier (MIS 12−8) and later (MIS 4−3) Neanderthal groups. In this context, Payre hominins would be expected to exhibit similar traits as coetaneous populations (such as Montmaurin-La Niche and BSV), more derived compared to MIS 8–12 hominins (such as SH and Arago) but primitive when compared to classic Neanderthals (such as La Quina, Regordou or Wezmeh). Over the

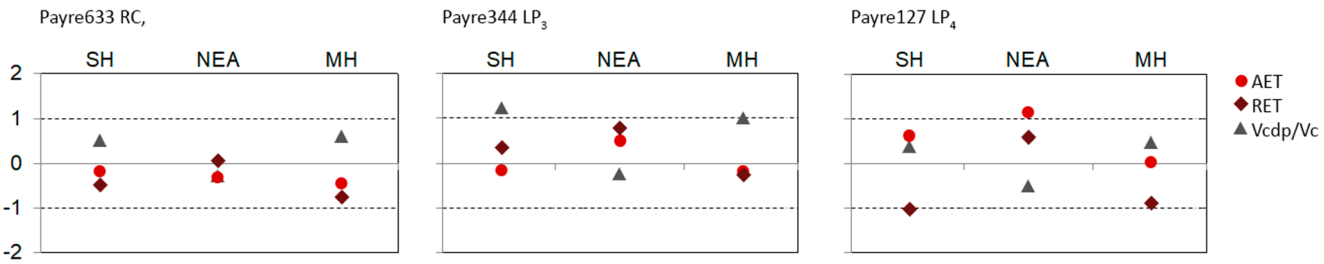

Fig. 8 Adjusted Z score of the 3D variables: AET (black circles), RET (red triangles) and percentage of dentine (green squares) assessed in Payre 14–633 (C,), Payre 8–344 (LP3) and Payre 6–127 (LP4) and compared to the variation expressed by Sima de los Huesos (SH), Neanderthals (NEA) and recent modern humans (RMH). The solid line passing through zero represents the mean, and the other two lines correspond to the estimated 95% limit of variation expressed for the two comparative samples

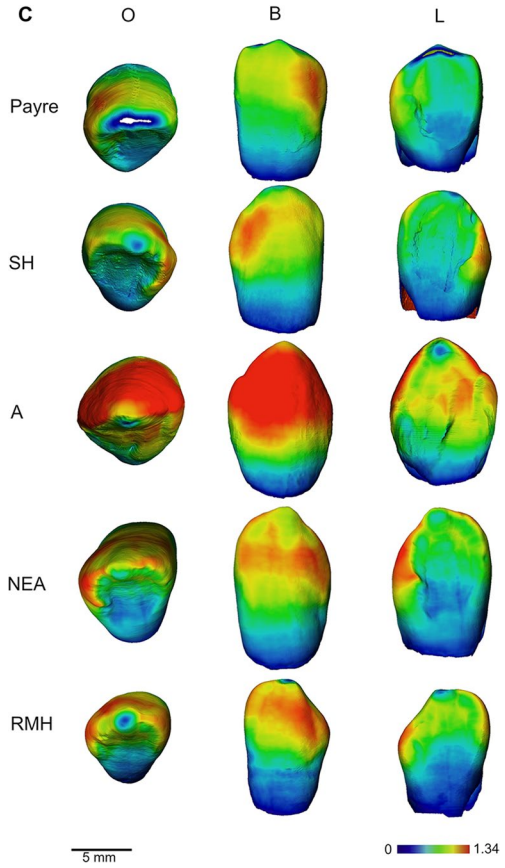

Fig. 9 Enamel thickness cartographies of the Payre 14–633 (RC,) and compared with those of Sima de los Huesos, Arago, Neanderthal and recent modern humans. Topographic thickness variation is rendered by a pseudo-color scale ranging from thinner dark-blue to thicker red. SH = Sima de los Huesos (AT-2783), A = Arago (A24), NEA = Neanderthal (Krapina D121) and RMH = recent modern human of European origin (UCM51). O = occlusal, B = buccal, L = lingual. (When needed specimens have been mirrored to the right to match the Payre specimen)

past decades, dental studies of European MP hominins have prompted alternative models for the Neanderthal evolution. The early Neanderthal sample from SH is dentally almost indistinguishable from later Neanderthals, with some traits expressed at even higher frequencies and degrees than in classic Neanderthals (e.g., Bermúdez de Castro et al. 2024a, b; Martínez de Pinillos 2017; Martínez de Pinillos et al. 2014; Martinón-Torres et al. 2012). In contrast, contemporaneous groups, such as Arago, are less derived and lack certain Neanderthal apomorphies (Bermúdez de Castro et al. 2019), while the sample from BSV (~350 ka) shows closer affinities to SH than to later Neanderthals (Martín-Francés et al. 2022). In this context, the "sink and source" model proposes that climatic fluctuations structured population dispersals and episodes of admixture, maintaining high interpopulation variability (Bermúdez de Castro and Martinón-Torres 2013; Dennell et al. 2011; MacDonald et al. 2012), extending the "ebb and flow" framework of Hublin and Roebroeks (2009). Consistent with this view, recent evidence of high phenotypic diversity among European MP groups followed by reduced variability in MIS 5 suggests demographic bottlenecks during the Late Pleistocene (Urciuoli et al. 2025). Together, the dental record underscores the importance of documenting variability within and between MP populations to clarify the evolutionary trajectory of the Neanderthal clade.

Since its discovery, multidisciplinary analyses of the deposits of Payre cave have provided a comprehensive understanding of the occupation. The cave was continuously occupied from MIS 8−7 to the end of MIS 6-beginning of MIS 5, as evinced by findings throughout the stratigraphic sequence, including species replacement from Neanderthals to *H. sapiens* (Grün et al. 2008; Moncel 2008; Valladas et al. 2008). Stable carbon and oxygen isotope values in herbivore teeth indicate climate stability in this region (Ecker et al. 2013), in contrast to the fluctuations occurring in other parts of Europe. In addition, Payre's proximity to diverse ecosystems (Moncel et al. 2002) suggests it may have acted as a refugium, influencing population dynamics. Palaeontological and archaeological analyses have allowed the reconstruction of this group hunting and technological strategies, showing that these human activities occurred locally within a 5–10/30 km radius (Baena et al. 2017; Bocherens et al. 2016; Fernandes et al. 2008; Moncel 2008; Rivals et al. 2009). Previous morphometric assessment of the dental remains by Moncel and Condemi (2007) and Condemi and Moncel (2008) already highlighted the similarities between the Payre sample and the Neanderthal clade. According to these studies, the Payre sample exhibits morphological and metric similarities with early Neanderthals as well as with later Neanderthals (Moncel and Condemi 2007). In order to test whether the Payre hominins (MIS 5–7) were characterized by distinct morphological features compared to earlier and later groups, for this study we have extended the temporal frame of the comparative sample, including early Neanderthal samples such as those from SH and Arago. We have also applied additional analytical approaches including the morphological description of the EDJ, GM of the EDJ ridge and enamel thickness characterization.

Our results demonstrate that the Payre dental assemblage captures the morphological variability documented within the Neanderthal lineage. Teeth from the lower stratigraphic levels display fewer derived Neanderthal features than those of the upper levels, suggesting either temporal differentiation within the site or coexistence of slightly distinct morphotypes. Despite this internal variability, the overall dental configuration of Payre aligns more closely with MP populations, particularly with the MIS 7 from Montmaurin-La

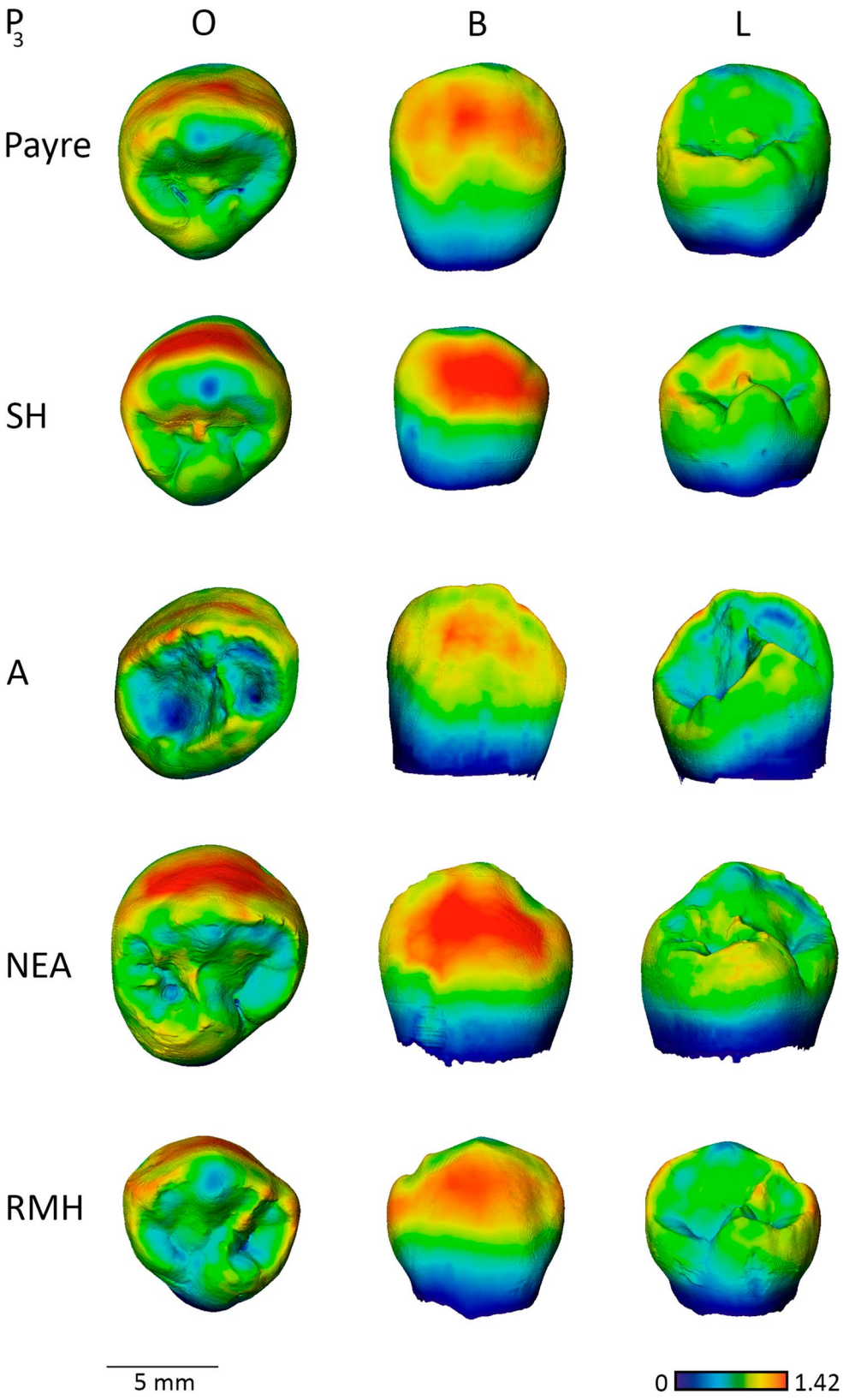

Fig. 10 Enamel thickness cartographies of the Payre 6–127 (LP_4) compared with those of Sima de los Huesos, Arago, Neanderthal and modern human. Topographic thickness variation is rendered by a pseudo-color scale ranging from thinner dark-blue to thicker red. SH = Sima de los Huesos (AT-3188), NEA = Neanderthal (Krapina D26), A = Arago (A28), and RMH = recent modern human of African origin (UCL141). O = occlusal, B = buccal, L = lingual. (When needed specimens have been mirrored to the left to match the Payre specimen)

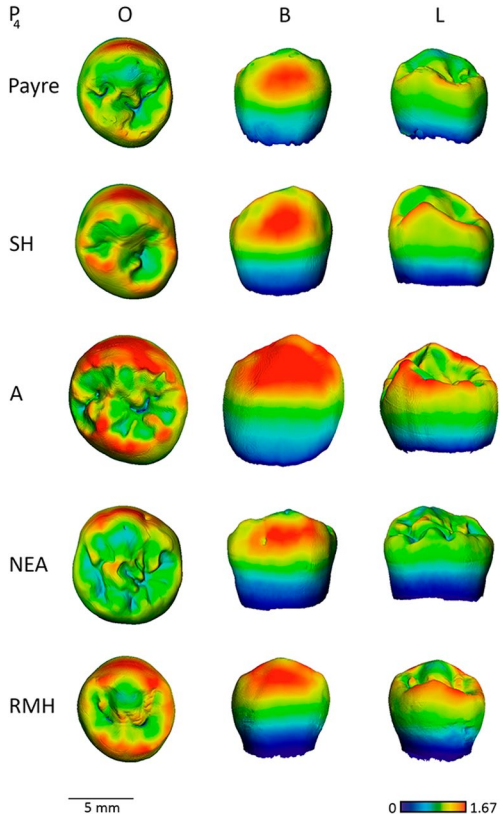

Fig. 11 Enamel thickness cartographies of the Payre 8–344 (LP_3) compared with those of Sima de los Huesos, Arago, Neanderthal and recent modern human. Topographic thickness variation is rendered by a pseudo-color scale ranging from thinner dark-blue to thicker red. SH = Sima de los Huesos (AT-4100), A = Arago (A71), NEA = Neanderthal (Krapina D111) and RMH = recent modern human of European origin (UCL67). O = occlusal, B = buccal, L = lingual. (When needed specimens have been mirrored to the left to match the Payre specimen)

Niche and BSV the earlier MIS 12 population from the SH, than with later Neanderthals (MIS 5 − 3).

These findings are consistent with previous assessments of the Payre material (Moncel and Condemi 2007; Condemi and Moncel 2008), which recognized its affinities with early and later Neanderthals. However, our results refine this interpretation by showing that Payre does not share a distinct set of traits exclusive to MIS7-5 Neanderthals. Instead, most features are widely distributed within the Neanderthal lineage. The affinities with SH are evident not only in crown morphology but also in EDJ rim configuration and enamel thickness. A similar enamel thickness pattern is also observed at Arago. Payre further shares traits with contemporaneous MIS 7 samples from BSV and Montmaurin-La Niche, although most of these traits (such as the morphology of the M_2 or the conformation of the EJD rim of the P^3) are also present in SH. The only feature uniquely shared between Payre and BSV is the morphological similarity between P^3s (Payre 13–717 and BSV specimen 3), although variability within the BSV assemblage has been documented (Martín-Francés et al. 2022).

In contrast, the Payre dental remains show weaker affinities with eastern European samples such as Mauer, Mala Balanica and Krapina, reinforcing a pattern of western European affinities. Our results also corroborate the conclusions of Verna and colleagues (2020) for Payre 15 (level Ga-MIS 7), a mandibular fragment whose morphology shows closer affinities to the SH sample than with later (MIS 6 − 3) Neanderthals, particularly in corpus thickness, anterior symphysis morphology and the mylohyoid line position. The only discrepancy concerns the comparison with Montmaurin-La Niche, which differs from Payre 15 in features such as the position of the lateral prominence and mental foramen as well as the relative corpus height.

Although the Payre sample remains small, most dental classes are represented by a single specimen, its variability is noteworthy. Three teeth (Payre 237-I_2, 250-I_1, and 633-C,) exhibit less derived Neanderthal morphology, emphasizing the mosaic character of the assemblage. If Payre functioned as a climatic refugium during MIS 7, as previously suggested by Eckhert et al. 2013; Moncel et al. 2019; this variability may reflect localized demographic dynamics, including small-scale admixture between the long-term southern residents and incoming groups retreating from harsher northern environments. In this context, Payre documents the persisted of regional variability within the Neanderthal clade during the MP.

Conclusion

In this article, we have reassessed the Payre dental remains to evaluate its position within the Neanderthal variability and to determine whether it can be differentiated from earlier groups, such as SH and Arago, or from later classic Neanderthals. We also examined potential variability across stratigraphic levels. Our results indicate that the Payre sample shows closer affinities to MIS 7 samples from BSV and Montmaurin-La Niche than to later Neanderthals (MIS 5 − 3). However, the traits observed in Payre are also widely shared with the earlier SH population. At the same time, the Payre sample exhibits internal variability throughout the sequence. The less derived, or less Neanderthal-like, morphology is observed in the anterior dentition and is restricted to specimens from the lower stratigraphic levels. Rather than representing a linear stage between earlier and later Neanderthals, the Payre dental record documents morphological variability within the Neanderthal clade, contributing to a broader understanding of regional differentiation in the MP.

Supplementary Information The online version contains supplementary material available at https://doi.org/10.1007/s12520-026-02453-1.

Acknowledgements We are grateful to the scientific and archaeological teams for their dedication to the recovery of the fossil teeth included in this study. We thank the CENIEH technicians from the Conservation and Restoration and the Microscopy and Micro-Computed Tomography Laboratory for their assistance during the scanning process. The comparative sample, including SH and modern humans, were scanned at CENIEH-ICTS facilities.

Author contributions L.M-F, M. M-P, M-H. M wrote the main manuscript text. M. M-T, A. V and C. G-C contributed to the writing of the main manuscrit text A.V., J. BdC, JL A, M. M-T and L.M-F funding acquisition. All authors reviewed the manuscript.

Funding Open Access funding enabled and organized by CAUL and its Member Institutions. This study was partially supported by the Regional Archaeology Service of the Auvergne-Rhône-Alpes region and the department of Ardèche (S.E. france). This study is also supported by the Horizon Program-Marie Sklodowska-Curie Actions of the EU Ninth programme (2021–2027) under the HORIZON-MSCA-2021-PF-01-Project: 101060482; The Spanish Ministry of Science and Innovation and European Regional Development Fund "ERDF A way of making Europe" (projects PID2021-122355NB-C31, PID2021-22355NB-C33) and PID2024-156477NB-C32 financed by MICIU/AEI/10.13039/501100011033/FEDER, UE. L.M-F receives funding from the EU-Horizon Program-Marie Sklodowska-Curie Actions of the EU Ninth programme (2021–2027) under the HORIZON-MSCA-2021-PF-01-Project: 101060482. M.M.P. has the support of the European Research Council within the European Union's Horizon Europe (ERC-2021-ADG, Tied2- Teeth, project number 101054659). M.M-T. receives funding from The Leakey Foundation through the personal support of D. Crook. C.G-C. receives funding through the Convocatoria 2024 de ayudas a Proyectos de I+D para doctores emergentes at the Universidad Autónoma de Madrid, financed by the Comunidad de Madrid (Grant No. SI4/PJI/2024−00104).

Data availability No datasets were generated or analysed during the current study.

Declarations

Competing interests The authors declare no competing interests.

References

Arsuaga JL, Martínez I, Arnold LJ, Aranburu A, Gracia-Téllez A, Sharp WD, Quam RM, Falguères C, Pantoja-Pérez A, Bischoff J, Poza-Rey E, Parés JM, Carretero JM, Demuro M, Lorenzo C, Sala N, Martinón-Torres M, García N, Alcázar de Velasco A, Cuenca-Bescós G, Gómez-Olivencia A, Moreno D, Pablos A, Shen C-C, Rodríguez L, Ortega AI, García R, Bonmatí A, Bermúdez de Castro JM, Carbonell E (2014) Neandertal roots: cranial and chronological evidence from Sima de los Huesos. Science 344:1358–1363

Arsuaga JL, Martínez I, Gracia A, Lorenzo C (1997) The sima de los huesos crania (Sierra de Atapuerca, Spain). A comparative study. J Hum Evol 33:219–281

Baena J, Moncel M-H, Cuartero F, Chacón Navarro MG, Rubio D (2017) Late middle Pleistocene genesis of Neanderthal technology in Western Europe: the case of Payre site (south-east France). Quatern Int 436:212–238

Bailey SE (2002) A closer look at Neanderthal postcanine dental morphology: the mandibular dentition. Anat Rec 269:148–156

Bailey SE (2004) A morphometric analysis of maxillary molar crowns of Middle-Late Pleistocene hominins. J Hum Evol 47:183–198

Bailey SE, Lynch JM (2005) Diagnostic differences in mandibular P4 shape between Neandertals and anatomically modern humans. Am J Phys Anthropol 126:268–277

Bayle P, Le Luyer M, Brown R, K.A (2017) The Palomas dental remains: enemal thickness and tissues proportions. In: Trinkaus E, Walker MJ (eds) The people of Palomas: neandertals from the Sima de las Palomas del Cabezo Gordo, Southeastern Spain. A&M University Anthropology Series, College Station, Texas., pp 115–137

Benazzi S, Panetta D, Fornai C, Toussaint M, Gruppioni G, Hublin J-J (2014) Technical note: guidelines for the digital computation of 2D and 3D enamel thickness in hominoid teeth. Am J Phys Anthropol 153:305–313

Bermúdez de Castro JM, Martinón-Torres M (2013) A new model for the evolution of the human Pleistocene populations of Europe. Quatern Int 295:102–113

Bermúdez de Castro JM, Martinón-Torres M, Martínez de Pinillos M, García-Campos C, Modesto-Mata M, Martín-Francés L, Arsuaga JL (2019) Metric and morphological comparison between the Arago (France) and Atapuerca-Sima de los Huesos (Spain) dental samples, and the origin of Neanderthals. Quat Sci Rev 217:45–61

Bermúdez de Castro JM, Martínez de Pinillos M, Martín-Francés L, Modesto-Mata M, García-Campos C, Arsuaga JL, Martinón-Torres M (2024a) Dental remains of the Middle Pleistocene hominins from the Sima de los Huesos site (Sierra de Atapuerca, Spain): mandibular dentition. Anat Rec 307:2394–2409

Bermúdez de Castro JM, Martínez de Pinillos M, Martín-Francés L, Modesto-Mata M, García-Campos C, Arsuaga JL, Martinón-Torres M (2024b) Dental remains of the Middle Pleistocene hominins from the Sima de los Huesos site (Sierra de Atapuerca, Spain): maxillary dentition. Anat Rec 307:2325–2342

Bocherens H, Díaz-Zorita Bonilla M, Daujeard C, Fernandes P, Raynal J-P, Moncel M-H (2016) Direct isotopic evidence for subsistence variability in middle Pleistocene Neanderthals (Payre, southeastern France). Q Sci Rev 154:226–236

Bookstein FL (1991) Morphometric tools for landmark data: geometry and biology. Cambridge University Press, Cambrige

Buti L, Le Cabec A, Panetta D, Tripodi M, Salvadori PA, Hublin J-J, Feeney RNM, Benazzi S (2017) 3D enamel thickness in Neandertal and modern human permanent canines. J Hum Evol 113:162–172

Carmignani L, Moncel M-H, Fernandes P, Wilson L (2017) Technological variability during the early middle palaeolithic in Western Europe. Reduction systems and predetermined products at the Bau de l'Aubesier and Payre (South-East France). PLoS One 12:e0178550

Cavillac C, Vialet A, Magne L, Grimaud-Hervé D, Valensi P, Moigne A-M, Bertrand B, Moncel M-H (2025) New late middle Pleistocene human remains at the Payre site (MIS 7, Ardèche, South-East France). J Hum Evol 208:103761. https://doi.org/10.1016/j.jhevol.2025.103761

Compton T, Stringer C (2015) The morphological affinities of the middle Pleistocene hominin teeth from Pontnewydd Cave, Wales. J Quaternary Sci 30:713–730

Condemi S, Moncel MH (2008) Les restes humains. In: Moncel MH (ed) Le site de Payre Occupations humaines dans la vallée du Rhône à la fin du Pléistocène moyen et au début du Pléistocène supérieur. Mémoire XLVI de la Société préhistorique française, France, pp 131–151

Couture C, Hublin J-J (2005) Les Néandertaliens. In: Dutour O, Hublin J-J, Vandermeersch B (eds) Origine et Evolution des Populations Humaines. Comité des travaux historiques et scientifiques, Paris, pp 129–149

Daura J, Sanz M, Arsuaga JL, Hoffmann DL, Quam RM, Ortega MC, Santos E, Gómez S, Rubio A, Villaescusa L, Souto P, Mauricio J, Rodrigues F, Ferreira A, Godinho P, Trinkaus E, Zilhão J (2017) New middle Pleistocene hominin cranium from Gruta da Aroeira (Portugal). Proc Natl Acad Sci USA 114:3397–3402

Dean D, Hublin J-J, Holloway R, Ziegler R (1998) On the phylogenetic position of the pre-Neandertal specimen from Reilingen, Germany. J Hum Evol 34:485–508

Dennell RW, Martinón-Torres M, Bermúdez de Castro JM (2011) Hominin variability, climatic instability and population demography in Middle Pleistocene Europe. Quat Sci Rev 30:1511–1524

Ecker M, Bocherens H, Julien M-A, Rivals F, Raynal J-P, Moncel M-H (2013) Middle pleistocene ecology and Neanderthal subsistence: insights from stable isotope analyses in Payre (Ardèche, south-eastern France). J Hum Evol 65:363–373

Feeney RNM, Zermeno JP, Reid DJ, Nakashima S, Sano H, Bahar A, Hublin JJ, Smith TM (2010) Enamel thickness in Asian human canines and premolars. Anthropol Sci 118:191–198

Fernandes P, Raynal J-P, Moncel M-H (2008) Middle palaeolithic raw material gathering territories and human mobility in the southern Massif Central, France: first results from a petro-archaeological study on flint. J Archaeol Sci 35:2357–2370

García-Campos C, Martinón-Torres M, Martínez de Pinillos M, Modesto-Mata M, Martín-Francés L, Perea-Pérez B, Zanolli C, Bermúdez de Castro JM (2018b) Modern humans sex estimation through dental tissue patterns of maxillary canines. Am J Phys Anthropol 167:914–923

García-Campos C, Martinón-Torres M, Martín-Francés L, Martínez de Pinillos M, Modesto-Mata M, Perea-Pérez B, Zanolli C, Labajo González E, Sánchez Sánchez JA, Ruiz Mediavilla E, Tuniz C, Bermúdez de Castro JM (2018a) Contribution of dental tissues to sex determination in modern human populations. Am J Phys Anthropol 166:459–472

García-Campos C, Martinón-Torres M, Martín-Francés L, Modesto-Mata M, Martínez de Pinillos M, Arsuaga JL, Bermúdez de Castro JM (2019) Enamel and dentine dimensions of the Pleistocene hominins from Atapuerca (Burgos, Spain): a comparative study of canine teeth. C R Palevol 18:72–89

García-Campos C, Modesto-Mata M, Martinón-Torres M, Martínez de Pinillos M, Martín-Francés L, Arsuaga JL, Bermúdez de Castro JM (2020) Sexual dimorphism of the enamel and dentine dimensions of the permanent canines of the Middle Pleistocene hominins from Sima de los Huesos (Burgos, Spain). J Hum Evol 144:102793

Grün R, Aubert M, Joannes-Boyau R, Moncel M-H (2008) High resolution analysis of uranium and thorium concentration as well as U-series isotope distributions in a Neanderthal tooth from Payre (Ardèche, France) using laser ablation ICP-MS. Geochim Cosmochim Acta 72:5278–5290

Guipert G, de Lumley M-A, Tuffreau A, Mafart B (2011) A late Middle Pleistocene hominid: Biache-Saint-Vaast 2, North France. C R Palevol 10:21–33

Hanegraef H, Martinón-Torres M, Martínez de Pinillos M, Martín-Francés L, Vialet A, Arsuaga JL, Bermúdez de Castro JM (2018) Dentine morphology of Atapuerca-Sima de los Huesos lower molars: evolutionary implications through three-dimensional geometric morphometric analysis. Am J Phys Anthropol 166:276–295

Hardy BL, Moncel M-H (2011) Neanderthal use of fish, mammals, birds, starchy plants and wood 125–250,000 years ago. PLoS One 6:e23768

Hublin J.J. (2009) The origin of Neandertals. Proc Natl Acad Sci 106:16022–16027

Hublin J-J, Roebroeks W (2009) Ebb and flow or regional extinctions? On the character of Neandertal occupation of northern environments. CR Palevol 8:503–509

Kono RT (2004) Molar enamel thickness and distribution patterns in extant great apes and humans: new insights based on a 3-dimensional whole crown perspective. Anthropol Sci 112:121–146

Lateur N, Daujeard C, Fourvel J-B, Moncel M-H (2024) Evidence of bears exploitation by early Neanderthals at the middle pleistocene site of payre (MIS 8–6, Southeastern France). Q Sci Rev 332:108653

Macchiarelli R, Bayle P, Bondioli L, Mazurier A, Zanolli C (2013) From outer to inner structural morphology in dental anthropology: integration of the third dimension in the visualization and quatitative analysis of fossil remains. In: Scott GR, Irish JD (eds) Anthropological Perspectives on Tooth Morphology. Genetics, Evolution, Variation. Cambridge Iniversity, Cambridge, pp 250–277

MacDonald K, Martinón-Torres M, Dennell RW, Bermúdez de Castro JM (2012) Discontinuity in the record for hominin occupation in south-western Europe: Implications for occupation of the middle latitudes of Europe. Quatern Int 271:84–97

Martinón-Torres M, Bastir M, Bermúdez de Castro JM, Gómez A, Sarmiento S, Muela A, Arsuaga JL (2006) Hominin lower second premolar morphology: evolutionary inferences through geometric morphometric analysis. J Hum Evol 50:523–533

Martinón-Torres M, Bermúdez de Castro JM, Gómez-Robles A, Arsuaga JL, Carbonell E, Lordkipanidze D, Manzi G, Margvelashvili A (2007) Dental evidence on the hominin dispersals during the Pleistocene. Proc Natl Acad Sci USA 104:13279–13282

Martinón-Torres M, Bermúdez de Castro JM, Gómez-Robles A, Prado-Simón L, Arsuaga JL (2012) Morphological description and comparison of the dental remains from Atapuerca-Sima de los Huesos site (Spain). J Hum Evol 62:7–58

Martinón-Torres M, Martínez de Pinillos M, Skinner MM, Martín-Francés L, Gracia-Téllez A, Martínez I, Arsuaga JL, Bermúdez de Castro JM (2014) Talonid crests expression at the enamel–dentine junction of hominin lower permanent and deciduous molars. C R Palevol. https://doi.org/10.1016/j.crpv.2013.12.002

Martin RMG, Hublin JJ, Gunz P, Skinner MM (2017) The morphology of the enamel–dentine junction in Neanderthal molars: gross morphology, non-metric traits, and temporal trends. J Hum Evol 103:20–44

Martínez de Pinillos M (2017) Estudio y caracterización morfológica de los patrones de crestas del trigónido y talónido en el esmalte y en la dentina de los homininos del Pleistoceno de la Sierra de Atapuerca (Burgos)mediante técnicas de microtomografía computarizada. Compartiva con otros grupos humanos e inferencias evolutivas. Universidad de Burgos

Martínez de Pinillos M, Martinón-Torres M, Skinner MM, Arsuaga JL, Gracia-Téllez A, Martínez I, Martín-Francés L, Bermúdez de Castro JM (2014) Trigonid crests expression in Atapuerca-Sima de los Huesos lower molars: internal and external morphological expression and evolutionary inferences. C R Palevol 13:205–221

Martínez de Pinillos M, Martín-Francés L, de Castro JMB, García-Campos C, Modesto-Mata M, Martinón-Torres M, Vialet A (2020) Inner morphological and metric characterization of the molar remains from the Montmaurin-La Niche mandible: the Neanderthal signal. J Hum Evol 145:102739

Martín-Francés L, de Castro Bermúdez, Martínez de Pinillos JM, Martinón-Torres M, Arsuaga M, Bertrand JL, Vialet B, A (2022) Middle Pleistocene hominin teeth from Biache-Saint-Vaast, France. Archaeol Anthropol Sci 14:215

Martín-Francés L, Kamath S, Soligo C, Martínez de Pinillos M, Song X, Arsuaga JL, de Bermúdez JM, Martinón-Torres M (2025) Enamel thickness in Atapuerca-H. antecessor and Sima de los Huesos permanent premolars. Am J Biol Anthropol DOI.10.1002/ajpa.70068

Martín-Francés L, Martinón-Torres M, Martínez de Pinillos M, García-Campos C, Zanolli C, Bayle P, Modesto-Mata M, Arsuaga JL, de Bermúdez JM (2020) Crown tissue proportions and enamel thickness distribution in the Middle Pleistocene hominin molars from Sima de los Huesos (SH) population (Atapuerca, Spain). PLoS ONE 15(6):e0233281. 10.1371/journal.pone.0233281

Maureille B, Rougier H, Houet F, Vandermeersch B (2001) Les dents inférieures du Néandertalien Regourdou 1 (site de Regourdou, commune de Montignac, Dordogne): analyses métriques et comparatives. Paleo 13:183–200

Meyer M, Arsuaga J-L, de Filippo C, Nagel S, Aximu-Petri A, Nickel B, Martínez I, Gracia A, de Castro JMB, Carbonell E, Viola B, Kelso J, Prüfer K, Pääbo S (2016) Nuclear DNA sequences from the Middle Pleistocene Sima de los Huesos hominins. Nature 531:504–507

Meyer M, Fu Q, Aximu-Petri A, Glocke I, Nickel B, Arsuaga J-L, Martinez I, Gracia A, Bermudez de Castro JM, Carbonell E, Paabo S (2014) A mitochondrial genome sequence of a hominin from Sima de los Huesos. Nature. https://doi.org/10.1038/nature12788

Mitteroecker P, Bookstein F (2011) Linear discrimination, ordination, and the visualization of selection gradients in modern morphometrics. Evol Biol 38:100–114

Mitteroecker P, Gunz P, Windhager S, Schaefer K (2013) A brief review of shape, form, and allometry in geometric morphometrics, with applications to human facial morphology. Hystrix 24:59–66

Molnar S (1971) Human tooth wear, tooth function and cultural variability. Am J Phys Anthropol 34:175–189

Moncel MH (2008) Payre. Des occupations humaines de la moyenne vallée du Rhône de la fin du Pléistocène moyen et du début du Pléistocène supérieu. Mémoire de la Société Préhistorique Française, XLVI,, France

Moncel MH, Condemi S (2007) The human remains of the site of Payre (S-E France, MIS 7 – 5). Remarks on stratigraphic position and interest. Anthropologie (1962-) 45:19–30

Moncel M-H, Debard E, Desclaux E, Dubois J-M, Patou-Mathis M, Lamarque F, Vilette P (2002) Le cadre de vie des hommes du Paléolithique moyen (stades isotopiques 6 et 5) dans le site de Payre (Rompon, Ardèche): d'une grotte à un abri sous roche effondré. Bulletin de la Société préhistorique française, pp 249–273

Moncel M-H, Fernandes P, Willmes M, James H, Grün R (2019) Rocks, teeth, and tools: new insights into early Neanderthal mobility strategies in South-Eastern France from lithic reconstructions and strontium isotope analysis. PLoS One 14:e0214925

Olejniczak AJ, Smith TM, Feeney RNM, Macchiarelli R, Mazurier A, Bondioli L, Rosas A, Fortea J, de la Rasilla M, Garcia-Tabernero A, Radovcic J, Skinner MM, Toussaint M, Hublin J-J (2008) Dental tissue proportions and enamel thickness in Neandertal and modern human molars. J Hum Evol 55:12–23

Pedergnana A, Ollé A, Borel A, Moncel M-H (2018) Microwear study of quartzite artefacts: preliminary results from the Middle Pleistocene site of Payre (South-eastern France). Archaeol Anthropol Sci 10:369–388

Posth C, Wißing C, Kitagawa K, Pagani L, van Holstein L, Racimo F, Wehrberger K, Conard NJ, Kind CJ, Bocherens H, Krause J (2017) Deeply divergent archaic mitochondrial genome provides lower time boundary for African gene flow into Neanderthals. Nat Commun 8:16046. https://doi.org/10.1038/ncomms16046

Prüfer K, de Filippo C, Grote S, Mafessoni F, Korlević P, Hajdinjak M, Vernot B, Skov L, Hsieh P, Peyrégne S, Reher D, Hopfe C, Nagel S, Maricic T, Fu Q, Theunert C, Rogers R, Skoglund P, Chintalapati M, Dannemann M, Nelson BJ, Key FM, Rudan P, Kućan Ž, Gušić I, Golovanova LV, Doronichev VB, Patterson N, Reich D, Eichler EE, Slatkin M, Schierup MH, Andrés AM, Kelso J, Meyer M, Pääbo S (2017) A high-coverage Neandertal genome from Vindija Cave in Croatia. Science 358:655–658. https://doi.org/10.1126/science.aao1887

R Core Team (2024) R: a language and environment for statistical computing. R foundation for statistical computing, Vienna, Austria.

Richard M, Pons-Branchu E, Genuite K, Jaillet S, Joannes-Boyau R, Wang N, Genty D, Cheng H, Price GJ, Pierre M, Dapoigny A, Falguères C, Tombret O, Voinchet P, Bahain J-J, Moncel M-H (2021).= Timing of Neanderthal occupations in the southeastern margins of the Massif Central (France): A multi-method approach. Quat Sci Rev 273:107241. https://doi.org/10.1016/j.quascirev.2021.107241

Rivals F, Moncel M-H, Patou-Mathis M (2009) Seasonality and intra-site variation of Neanderthal occupations in the Middle Palaeolithic locality of Payre (Ardèche, France) using dental wear analyses. J Archaeol Sci 36:1070–1078

Roksandic M, Mihailović D, Mercier N, Dimitrijević V, Morley MW, Rakočević Z, Mihailović B, Guibert P, Babb J (2011) A human mandible (BH-1) from the Pleistocene deposits of Mala Balanica cave (Sićevo Gorge, Niš, Serbia). J Hum Evol 61:186–196

Rosas A, Bastir M, Martínez-maza C, García-Tabernero A, Lalueza-Fox C (2006) Inquiries into Neanderthal craniofacial development and evolution: "accretion" versus "organismic" models. In: Hublin J-J, Harvati K, Harrison T (eds) Neanderthals Revisited: New Approaches and Perspectives. Springer Netherlands, Dordrecht, pp 37–69

Schwartz GT, Dean MC (2005) Sexual dimorphism in modern human permanent teeth. Am J Phys Anthropol 128:312–317

Scolan H, Santos F, Tillier AM, Maureille B, Quintard A (2012) Des nouveaux vestiges néanderthaliens à Las Pélénos (Monsempron-Libos, Lot-et-Garonne, France). Bulletins et Mémoires de la Société d'Anthropologie de Paris 24:69–95

Skinner MM, de Vries D, Gunz P, Kupczik K, Klassen RP, Hublin J-J, Roksandic M (2016) A dental perspective on the taxonomic affinity of the Balanica mandible (BH-1). J Hum Evol 93:63–81

Slon V, Mafessoni F, Vernot B, de Filippo C, Grote S, Viola B, Hajdinjak M, Peyrégne S, Nagel S, Brown S, Douka K, Higham T, Kozlikin MB, Shunkov MV, Derevianko AP, Kelso J, Meyer M, Prüfer K, Pääbo S (2018) The genome of the offspring of a Neanderthal mother and a Denisovan father. Nature 561:113–116. https://doi.org/10.1038/s41586-018-0455-x

Smith TM, Austin C, Green DR, Joannes-Boyau R, Bailey S, Dumitriu D, Fallon S, Grün R, James HF, Moncel M-H, Williams IS, Wood R, Arora M (2018) Wintertime stress, nursing, and lead exposure

in Neanderthal children. Sci Adv. https://doi.org/10.1126/sciadv.aau9483

Urciuoli A, Martínez I, Quam R, Arsuaga JL, Keeling BA, Diez-Valero J, Conde-Valverde M (2025) Semicircular canals shed light on bottleneck events in the evolution of the Neanderthal clade. Nat Commun 16:972

Valladas H, Mercier N, Ayliffe LK, Falguères C, Bahain JJ, Dolo JM, Froget L, Joron JL, Masaoudi H, Reyss JL, Moncel MH (2008) Radiometric dates for the Middle Palaeolithic sequence of Payre (Ardèche, France). Quat Geochronol 3:377–389

Verna C, Détroit F, Kupczik K, Arnaud J, Balzeau A, Grimaud-Hervé D, Bertrand S, Riou B, Moncel M-H (2020) The Middle Pleistocene hominin mandible from Payre (Ardèche, France). J Hum Evol 144:102775

Vialet A, Modesto-Mata M, Martinón-Torres M, Martínez de Pinillos M, Bermúdez de Castro J-M (2018) A reassessment of the Montmaurin-La Niche mandible (Haute Garonne, France) in the context of European Pleistocene human evolution. PLoS One 13:e0189714

Zanolli C, Biglari F, Mashkour M, Abdi K, Monchot H, Debue K, Mazurier A, Bayle P, Le Luyer M, Rougier H, Trinkaus E, Macchiarelli R (2019) A neanderthal from the Central Western Zagros, Iran. Structural reassessment of the Wezmeh 1 maxillary premolar. J Hum Evol 135:102643

Zanolli C, Martinón-Torres M, Bernardini F, Boschian G, Coppa A, Dreossi D, Mancini L, Martínez de Pinillos M, Martín-Francés L, Bermúdez de Castro JM, Tozzi C, Tuniz C, Macchiarelli R (2018) The middle Pleistocene (MIS 12) human dental remains from Fontana Ranuccio (Latium) and Visogliano (Friuli-Venezia Giulia), Italy. A comparative high resolution endostructural assessment. PLoS One 13:e0189773